Northland: the climate of an Earth with a hemispheric continent

Marysa M. Laguë*

Department of Earth and Planetary Science, University of California Berkeley, Berkeley, CA, USA

Marianne Pietschnig

Department of Mathematics, University of Exeter, Exeter, United Kingdom

Sarah Ragen

School of Oceanography, University of Washington, Seattle, WA, USA

Timothy A. Smith

Oden Institute for Computational Engineering and Sciences, The University of Texas at Austin, Austin, TX, USA

David S. Battisti

Department of Atmospheric Sciences, University of Washington, Seattle, WA, USA

Corresponding author address: Marysa M. Laguë, Department of Earth and Planetary Science, University of California Berkeley, 307 McCone Hall, Berkeley, CA 94720.

E-mail: mlague@berkeley.edu

ABSTRACT

From a climate perspective, land differs from the ocean in several fundamental physical ways, including albedo, heat capacity, amount of water storage, and differences in resistance to evaporation. These differences alter the surface energy and water budgets over land compared to ocean, with implications for both surface climate and atmospheric circulation. In this study, we use an idealized general circulation model (Isca) to explore the climate state of Northland, a planet with a northern land hemisphere and a southern ocean hemisphere. These idealized simulations are motivated by the asymmetry of continental distribution on the globe, with a greater concentration of landmasses in the northern hemisphere and a larger area of ocean in the southern hemisphere, and further illuminate the basic role that land-sea contrasts play in global atmospheric dynamics. We find a much larger seasonal cycle of temperature over land compared to ocean, as expected. The continent is seasonally wet in the tropics, has a subtropical desert, and a moist high-latitude "swamp", where moisture transported from the tropics accumulates. Decreasing the land albedo leads to warming. In contrast to past studies, suppressing evaporation from the land surface cools the climate, resulting from decreased atmospheric water vapor and reduced trapping of longwave radiation, which dominates over the warming associated with reduced evaporative cooling at the surface. The ITCZ in the Northland simulations extends farther polewards over both the land and ocean hemispheres than the ITCZ in an aquaplanet. Our results demonstrate the potential for land and hemispheric asymmetries in controlling the large-scale axisymmetric atmospheric circulation.

1. Introduction

The physical properties of the land surface and the ocean differ in several fundamental ways. For instance, land has a much lower heat capacity than the ocean (Cess and Goldenberg 1981; North et al. 1983; Bonan 2008); land has a higher albedo than ocean (Budyko 1961, 1969; Payne 1972; Bonan 2008); the ocean has the ability to move heat laterally (Loft 1918; Richardson 1980; Trenberth and Caron 2001; Ferrari and Ferreira 2011; Forget and Ferreira 2019); and there are large climatic impacts of terrestrial orography (Queney 1948; Eliassen and Palm 1960; Manabe and Terpstra 1974; Held et al. 1985; McFarlane 1987). Moreover, land evaporates less water, and soil and vegetation properties provide resistance to evaporation over land (Manabe 1969; Bonan 2008, and references therein). The contrast between physical properties of land and ocean are important controls on atmospheric dynamics, profoundly impacting the climate. The hemispheric asymmetry in land-sea distribution has implications for global climate and the higher sensitivity of the Northern Hemisphere to increases in anthropogenic greenhouse gases (Manabe et al. 1991; Stouffer et al. 1989). In this study, we focus on how the limited capacity of the land to hold water and its higher albedo alter the climate system.

The albedo of different land types is much higher than that of ice-free ocean. Land albedo ranges from 0.05-0.25 (vegetated) to 0.5-0.9 (glaciers and snow) (Wiscombe and Warren 1980; Oke 1987; Bonan 2008). In contrast, the surface albedo of the ice-free ocean is generally less than 0.1 (Jin et al. 2004). The difference in top-of-atmosphere (TOA) albedo between land and ocean is less drastic, with TOA albedo ranging from 0.25 to 0.6 over snow-free land, and 0.1 to 0.5 over ice-free ocean for Earth in the present climate. These higher values result atmospheric controls on the TOA albedo, via the effects of cloud cover, aerosols, and attenuation (Donohoe and Battisti 2011).

Additionally, the land has a much smaller heat capacity than the ocean, and a limited ability to move energy laterally. Oceans can absorb large amounts of energy (Kuhlbrodt and Gregory 2012; Cheng et al. 2017) and transport energy via ocean currents, which means that there are areas of the ocean that can continually take up energy, while other regions act as a source of energy to the atmosphere (e.g. Marshall and Zanna 2014; Forget and Ferreira 2019). In contrast, energy absorbed at one location on land must be released back to the atmosphere at that same location in the form of upwards longwave radiation, sensible heat, or latent heat (evaporation). While the land can store energy on seasonal timescales, the annual mean heat storage of a land surface in equilibrium is near-zero (Milly and Shmakin 2002), and the seasonal storage of heat by the land surface is much smaller than that of the ocean (Marshall and Plumb 2008).

The limited capacity of the land surface to hold water and increased resistance to evaporation over land surfaces compared to over open water drastically alters evaporative fluxes over land. Over the ocean, evaporation is determined mainly by the conditions (e.g. the surface temperature and atmospheric humidity) at the atmosphere-ocean interface. In contrast, dry land surfaces have little water available for evaporation, and thus little evaporation occurs relative to the evaporative demand of the overlying atmosphere. Various properties of soil and vegetation further modulate the availability of water to the atmosphere, including total leaf area and roots that can provide access to water deep in the soil column (Canadell et al. 1996; Bonan 2008). Moreover, vegetation directly regulates the movement of water from the land to the atmosphere by opening and closing their stomata (small pores on leaves which modulate gas exchange) (Sellers et al. 1996).

These fundamental physical differences between land and ocean result in very different surface-atmosphere interactions. Changes in these land surface properties can modify the global climate system (Charney 1975; Shukla and Mintz 1982; Sud et al. 1988; Davin et al. 2010; Laguë et al. 2019). Large hemispheric energy imbalances, such as those generated by sea ice, large-scale

vegetation change, or an idealized energy source can drive large-scale changes in the Hadley circulation (Chiang and Bitz 2005; Broccoli et al. 2006; Kang et al. 2008; Swann et al. 2012; Laguë and Swann 2016; Kang 2020). In response to a hemispheric energy imbalance, the rising branch of the Hadley circulation moves towards the energy-rich hemisphere, thereby moving energy from the energy-rich hemisphere towards the energy-poor hemisphere and shifting the ITCZ towards the energy-rich hemisphere (Donohoe et al. 2013), provided there are no large changes in gross moist stability (see Geen et al. 2020, and references therein).

In this study, we use an idealized general circulation model configuration to explore how fundamental differences between the land and ocean affect the climate. To do this, we model the climate of a hypothetical planet that is Earth-like in size and orbital configuration, but has a continent covering the entire northern hemisphere, and an ocean covering the entire southern hemisphere. We explore the mean state of this planet, which we call Northland, and probe how modifying the albedo and capacity to hold water of the land surface alter the planet's climate. We also explore the climate of a similar, land-covered planet.

Idealized models are a useful tool in climate modeling as they help to narrow the gap between simulating the climate system and understanding its mechanisms, as highlighted in Sellers (1969), Held (2005), Jeevanjee et al. (2017), and Maher et al. (2019). Idealized models can be traced back to 'Galilean' idealizations, in which a problem is simplified to make it easier to solve (McMullin 1985). These simplified models are ideal limits. While an idealized model sacrifices realistic representations of physical processes, this approach aides in illuminating fundamental processes of the climate system (Levins 1966) - in this case, differences between land and ocean surface interactions with the atmosphere.

This study explores the climate of an idealized limit of the Earth system. At present, 68% of land on Earth is in the Northern Hemisphere and 32% is in the Southern Hemisphere. The hemispheric

asymmetry in the distribution of land is the primary cause of the hemispheric asymmetry in mean surface temperature, sea surface temperature, and zonal mean precipitation (Croll 1870; Frierson et al. 2013; Kang et al. 2015). Moreover, there are differing responses between the hemispheres to orbital forcing (Roychowdhury and DeConto 2019) and greenhouse gas forcing (Stouffer et al. 1989; Manabe et al. 1991).

The hemispheres experience the same distribution of incoming shortwave radiation at the top of the atmosphere (TOA) (Philander et al. 1996). Hemispheric asymmetry in absorbed solar radiation is due to the hemispheric asymmetry in the distribution of albedo (Stephens et al. 2008; Trenberth and Fasullo 2009), while hemispheric asymmetry in outgoing longwave radiation is mainly due to hemispherically asymmetric surface temperature and cloud distributions (Lindzen et al. 2001; Trenberth and Fasullo 2009). How much of the difference in climatology between the hemispheres can be attributed to the uneven distribution of the continents?

The distribution of land impacts climate in myriad ways, including by directing storm tracks, shaping ocean circulation, generating planetary waves, and impacting orographic forcing and diabatic heating of the atmosphere (Eliassen and Palm 1960; Hartmann 1994; Donohoe et al. 2020). In this study we investigate the fundamental differences in atmospheric dynamics and climate over land and ocean, as well as the climatic implications of the asymmetry in the distribution of land between the southern and northern hemispheres.

2. Methods

a. Model

In this study, we use Isca (Vallis et al. 2018), an idealized general circulation model (GCM) to explore the climate of an Earth-like planet with an idealized continental configuration. The

atmosphere is coupled to a 20m slab ocean without any ocean heat transport. Land gridcells differ from ocean gridcells by having a higher albedo, smaller heat capacity, a finite reservoir of water, and a parameterized representation of soil that reduces the rate of evaporation when the soil is less than saturated. The land parameterization used in this study is similar to that of Manabe (1969), where land hydrology is represented using a bucket model. There is no snow or sea ice.

The atmosphere uses moist dynamics, but does not represent clouds. While cloud responses to land surface properties and their changes can play an important role in determining impacts on surface climate (Cho et al. 2018; Sikma and Vilà-Guerau de Arellano 2019; Laguë et al. 2019; Kim et al. 2020), cloud responses to climate perturbations are also a large source of uncertainty (Stocker et al. 2013; Zelinka et al. 2017). Our idealized modeling framework avoids uncertainties associated with cloud responses to climate perturbations, at the cost of not capturing any cloud interaction effects. The surface albedo α of both water ($\alpha_{ocean} = 0.25$) and land ($\alpha_{land} = 0.325$; table 1) is higher than it would be in a model that included clouds, to allow for a more realistic planetary albedo at the top of the atmosphere (Donohoe and Battisti 2011). Despite the absence of clouds, the model *does* produce precipitation (see Vallis et al. 2018, for details). Simulations are run using a T42 horizontal resolution (roughly 2.8° latitude by 2.8° longitude) with 40 vertical levels.

b. Experiments

We run a total of 7 simulations, with two continental configurations and various land surface properties modified between simulations (table 1). In all simulations, there is a seasonal cycle in insolation (obliquity = 23.439 degrees, eccentricity = 0) with a 360 day year; atmospheric CO_2 concentrations are fixed at 300 ppm.

In each of the first four simulations described, the bottom boundaries in the northern and southern hemispheres (NH and SH, respectively) of the planet are prescribed as land and ocean, respectively. We refer to simulations with this continental configuration as "NorthlandXX" (where "XX" indicates a specific simulation). Our "control" simulation (to which we generally compare our other experiments) is "NorthlandBright". In NorthlandBright, the NH continent has an albedo that is 1.3 times that of the ocean ($\alpha_{land} = 0.325$, $\alpha_{ocean} = 0.25$). The heat capacity of the land is 1/10 that of the ocean (i.e. equivalent to a 2m mixed layer ocean). The roughness length is 0.2 mm, and is uniform over land and ocean in our simulations. Hydrology is represented as a bucket model, where the capacity of the land to hold water is 150 mm ("bucket capacity"), and water on land is initialized everywhere at 100 mm. The bucket receives (loses) water when there is more (less) precipitation than evaporation. If the bucket reaches capacity, any excess precipitation is treated as 'runoff'. When the bucket is more than 3/4 full, the resistance to evaporating water from the land surface is the same as over open water (Manabe 1969; Vallis et al. 2018).

We run three additional Northland experiments to demonstrate various aspects of the land surface's impact on the climate system. In each of these simulations, a single property of the land surface is modified compared to NorthlandBright. In the "NorthlandDark" experiment, the albedo of the land is reduced so that it is the same as the ocean ($\alpha_{land} = \alpha_{ocean} = 0.25$). In the "NorthlandEmpty" experiment, the land surface is initialized with no water on the land surface, thus, all water that ends up on land must have originated from the ocean. NorthlandEmpty differs from NorthlandBright only in the initial conditions. In the "NorthlandDry" experiment, the capacity of the land to hold water is greatly reduced, to near-zero (0.01 mm). This effectively shuts off evaporation from the land surface.

In addition to the four Northland simulations, we run two simulations where the entire planet is covered with land. The first all-land experiment ("Landworld") has the same land properties

as NorthlandBright: the albedo is $\alpha_{land} = 0.325$, and the bucket has a fixed capacity (150 mm). Since there is no ocean on Landworld, the runoff term (i.e. precipitation onto a full bucket) is discarded, meaning that this simulation *does not conserve water*. In the second all-land experiment ("Lakeworld"), the bucket hydrology of the land model is modified to allow the bucket at each gridcell to hold an unlimited amount of water. That is, if the amount of water in the bucket exceeds the bucket capacity, the water is *kept* in that gridcell; there is no runoff. This differs from an ocean gridcell because the land in Lakeworld must get its water from precipitation - water is not unlimited. Each gridcell is initialized with 100mm of water, and as the simulation moves forwards in time buckets can empty via evaporation or fill up via precipitation. Conceptually, this allows the land surface to form lakes in regions where precipitation exceeds evaporation. Note, however, that the lack of topography means these "lakes" are the size and shape of a model gridcell, and their location is determined by atmospheric moisture transport and is not impacted by river routing. In contrast to Landworld, Lakeworld conserves water.

Lastly, we run an aquaplanet simulation ("Aqua") with no land, where the whole planet is covered with a 20m deep mixed layer slab ocean, with an albedo of $\alpha_{ocean} = 0.25$.

Simulations are run for a total of 50 years (with the exception of Landworld and Lakeworld, which are run for 80 years, given the unique water cycles of the all-land simulations). The first four years are discarded to allow for model spin-up, after which time there is a global-mean drift in surface temperatures of less than 0.01 K/year in the Northland and Aqua simulations (figure S1). The Landworld and Lakeworld simulations do not reach equilibrium in 80 years. Water is not conserved in Landworld, but perhaps an equilibrium would eventually be reached after either all the water was lost from the system, or after the system reached a state where there were no regions where precipitation exceeded evaporation (and thus no additional water would be discarded as

'runoff'). These two simulations are used to demonstrate the transient migration of water, rather than explored for their equilibrium climates.

When statistical significance is shown for a difference between two experiments, a student's t-test is used, with $p < 0.05$ indicating 95% confidence that the simulations differ significantly. When error bars are used, they represent $\pm$ 1 standard deviation.

3. Results

We investigate how different properties of the land and ocean modify temperatures (section a), the water cycle (section b), atmospheric circulation (section c) and ITCZ location (section d). In each of those four sections we begin by describing the climate of our control simulation (NorthlandBright), then study how land albedo (NorthlandDark) and evaporative resistance (NorthlandDry) impact the climate of our idealized planet. We also study the water cycle in Landworld and Lakeworld, and the ITCZ location in the absence of land (Aqua).

NorthlandBright can be divided into four distinct climatic zones: the SH ocean, the seasonally wet tropical land belt, the NH mid-latitude desert, and the NH moist polar region. There is a stark contrast in the seasonal cycle of temperature and rainfall between the NH continent and the SH ocean.

a. Temperature

(I) CLIMATOLOGY

The mean climate of the NorthlandBright simulation reflects a world where the area-weighted annual mean surface temperature over the continent is slightly cooler (281K) than over the ocean (283K) (figure S2a, table S1); this is unlike present-day Earth, where extra-tropical land regions are generally warmer than extra-tropical ocean regions (Wallace et al. 1995; Sutton et al. 2007).

However, the continent has a much larger seasonal cycle of temperature than the ocean, reflecting its smaller heat capacity (figure S2b, table S1). The hottest part of the continent, with temperatures reaching 304 K, occurs around 30°N during NH summer, while temperatures near the north pole plunge to 220K during NH winter (figure 1a). Temperatures and seasonality over the SH ocean are much more moderate, with a mean temperature difference of only 4 K between summer and winter, compared to a mean seasonal cycle of 33 K in the NH (figure S2b, table S1).

(II) Temperature response to land albedo

In NorthlandDark, the land albedo is the same as that of the ocean. As such, the land hemisphere absorbs more solar energy in NorthlandDark than in NorthlandBright, leading to warmer temperatures year-round (figures 1c). Excess shortwave energy absorbed by the NH must be re-released to the atmosphere either as emitted longwave radiation, sensible heat, or latent heat - all of which increase in NorthlandDark (figures 2, 3). Increased evaporation and greater air temperatures lead to more atmospheric water vapor in the NH in NorthlandDark (figure 1e), in turn leading to more downwelling longwave radiation at the surface (figure 3b). NorthlandDark is warmer than NorthlandBright at all latitudes, over both land and ocean, due to the ability of the atmosphere to mix water vapor and heat (figure 1c). Surface temperatures over the ocean hemisphere are on average 3K warmer than in NorthlandBright, but are in excess of 10K warmer over the northern (land) hemisphere mid-latitudes. The warming signal over the land hemisphere is largest in summer, but exists year round (figures 1c, S2, table S1).

(III) Temperature response to land evaporation

In NorthlandDry, evaporation from the land surface is suppressed. With all else held equal (i.e. the same amount of incoming energy to the land surface, the same water availability, etc.), this

reduction in evaporation from the land surface should lead to greater surface temperatures. In the absence of evaporative cooling, the absorbed energy at the surface must be emitted in the form of sensible heat or longwave radiation, both of which require an increase in surface temperatures. Indeed, both Shukla and Mintz (1982) and Laguë et al. (2019) find that reducing evaporation from the land surface leads to surface warming. In contrast to these past studies however, we find that NorthlandDry is cooler than NorthlandBright (figures 1c, S2, table S1). Globally, surface temperatures in NorthlandDry are 6 K cooler than in NorthlandBright (table S1). The decrease in atmospheric water vapor due to reduced evaporation from the land surface cools NorthlandDry relative to NorthlandBright (figure 1f). Since water vapor is a strong greenhouse gas, downwelling longwave radiation is greatly reduced (figure 3g). The reduction in downwelling longwave radiation exceeds the reduction in latent heat flux (which would otherwise lead to warming). The reduction in downwelling longwave radiation reaches 175 W/m^2 in the northern high latitudes, while the reduction in latent heat flux peaks at around 80 W/m^2, with the largest reductions in the northern tropics and high latitudes. In the dry subtropics, latent heat flux is already near-zero for most of the year in NorthlandBright, so suppressing evaporation has little impact on latent heat flux in this region. The net effect is a land surface with less net incoming energy at the surface in NorthlandDry than NorthlandBright (figure 2), and thus much cooler surface temperatures in all seasons in NorthlandDry compared to NorthlandBright. The cold anomaly is fairly homogeneous over the ocean hemisphere, but it is amplified at the pole in the NH year-round, with particularly large cold anomalies in the northern mid-latitudes during JJA (figure 1c). Note that there is actually a slight increase in downwelling shortwave radiation at the surface over land during NH summer months (due to reduced absorption of shortwave radiation by water vapor). However, the decrease in downwelling longwave radiation from reduced longwave trapping by water vapor dominates the change in absorbed surface energy (figures 2, 3).

b. Water cycle

(I) CLIMATOLOGY

The globally averaged annual mean rainfall in the NorthlandBright simulation is approximately 2 mm/day. Unsurprisingly, more of this rain falls over the ocean (2.9 mm/day) than over the continent (1.5 mm/day), with a strong latitudinal dependence (figure 1b, table S1). The ITCZ has a strong seasonal cycle, with heavier rainfall and a substantially farther polewards peak over the ocean than over the continent (figure 1b, 4a). Over the continent, the ITCZ reaches its farthest northwards extent during August and September, with the peak in precipitation reaching approximately 15°N. In contrast, the peak in the ITCZ over the ocean occurs at around 20°S during March, with roughly double the rate of precipitation in the ocean ITCZ-peak than the land ITCZ-peak. The land cannot support as strong an ITCZ as all the moisture for the ITCZ must initially be brought onto the land each season by ITCZ precipitation; in contrast, the ocean provides an unlimited supply of water in the form of nearby evaporation that can subsequently be precipitated in the SH ITCZ.

In NorthlandBright, moist air is transported from the ocean onto the continent, where it rains out in the tropics. Terrestrial tropical precipitation is at its most intense from August to November. The land water evaporates quickly in the hot tropics (i.e. evaporation has a similar seasonal cycle to precipitation; figure 4a,b). North of 20°N, precipitation is roughly equal to evaporation in the annual mean (figure S3). Despite heavy wet-season precipitation in the tropics, the ground between 0-20°N dries out during the dry season (February-June), because of the strong seasonal evaporation (figures 1b, 4b,d, 5a, 3e).

In the northern subtropics there is a desert (from roughly 20-40°N), where the soil is very dry year-round (figures 1b, 4 d). A small amount of precipitation falls over this desert region during the tropical wet season (figures 4a, 5a, S4).

The extratropical maximum in precipitation at about 40S in the ocean hemisphere is storm track precipitation associated with baroclinic cyclones (figure 1c). Precipitation in the ocean hemisphere storm track is nearly seasonally invariant. In contrast, extratropical precipitation in the land hemisphere features a broad maximum in summertime that extends from 50°N to the pole that is likely due to localized convection. As in the ocean hemisphere, the peak is wintertime precipitation in the land hemisphere is associated with the mid-latitude storm track, maximizing at 40°N, but the peak is damped due to the absence of a water vapor source (i.e. an ocean).

The high latitude soil is moist year-round, forming what we call the "Great Northern Swamp". In the Great Northern Swamp, soils are saturated with moisture for much of the year, with slightly less terrestrial water storage during July-September when evaporation (fueled by increased summer insolation) exceeds precipitation (figure 4c). The soil moisture in the Great Northern Swamp is supplied by water transport from the tropics, and not – as might be expected – from local moisture recycling alone. When the land is initialized without any water (NorthlandEmpty), the high latitude soil water is indistinguishable from NorthlandBright within 4-5 years (figures 4d-e, S5). The transport of water to the poles is explored further in sub-section IV.

(II) Water cycle response to land albedo

NorthlandDark is not only warmer than NorthlandBright - it is also wetter. In the tropics, the ITCZ shifts equatorward during SH summer (DJF), and the ITCZ intensifies during NH summer (JJA) (figures 1d, 5b)). Precipitation changes outside of 30°S-30°N are small. These shifts in the ITCZ are associated with hemispheric energy imbalances are discussed further in section 3.

(III) Water cycle response to land evaporation

The response of precipitation to suppressed terrestrial evaporation in the NorthlandDry experiment is widespread. There is a clear intensification and narrowing of the ITCZ during DJF in the SH in the NorthlandDry experiment compared to NorthlandBright (figure 1d). Precipitation over the continent decreases almost to zero, though a very weak ITCZ still generates a small amount of precipitation over the southern edge of the continent in August-October (figures 1d, 5c). The behaviour of the ITCZ due to suppressed evaporation is discussed further in section c.

(IV) Landworld and Lakeworld

In all the Northland simulations except NorthlandDry (which can't store water on land), a Great Northern Swamp forms in the northern high latitudes. In the absence of a large low-latitude water source, is the Great Northern Swamp sustainable? To address this question, we explore two all-land simulations, Landworld and Lakeworld. Both simulations have no ocean; land surface properties are similar to those in NorthlandBright and are initialized with 100 mm of water at every gridcell. Landworld has a fixed bucket capacity of 150mm, while Lakeworld can form lakes of arbitrary depth at all gridcells.

Within a few years, the water in both Landworld and Lakeworld has all been transported to the polar high latitudes (figure 4f,g). Landworld does not conserve water, since runoff is discarded when bucket capacity is exceeded. Thus, the atmosphere becomes increasingly drier in the Landworld simulation, while the polar swamps retreat polewards and slowly disappear (figure 4f). This behaviour is not physically realistic; thus, we next consider the Lakeworld simulation, where water *is* conserved.

In Lakeworld, if more water exists on a terrestrial gridcell than the bucket capacity, a lake forms. Water evaporates from the lake with no resistance associated with soil; if the volume of water

in a gridcell decreases below the soil's capacity to hold water, the standard representation of soil evaporation is used. That is, it is more difficult to evaporate water when the bucket is less than 3/4 full, where "full" is 150mm (despite more than 150mm of water being allowed to pool in the gridcell). Lakeworld rapidly forms two lakes, one over each pole (figure 4g), which deepen as the simulation progresses. The lake edge retreats polewards quickly over the first 35 years, then slower as the simulation progresses. In effect atmospheric circulation redistributes water to concentrate it in the polar regions; the atmosphere of Lakeworld is very dry, with atmospheric moisture isolated to the lower troposphere near the poles (figure S6). Surface temperatures in Lakeworld are above 0°C year round in the lower latitudes, and at higher latitudes during summer (figure S7).

c. Circulation

(I) CLIMATOLOGY

As with the real Earth, our Northland simulations receive the most insolation in the tropics, and atmospheric circulation acts to move energy from the tropics to the high-latitudes where it is radiated to space. To quantify the excess (or deficit) of energy being absorbed by the atmosphere at any latitude, we calculate the net downward flux of energy at the top of the atmosphere (TOA_{net}) and at the surface (SFC_{net}), and define their difference as the atmospheric column energy source F_{net} (equations 1-3).

$$TOA_{net} = SW^{\downarrow}_{TOA} - SW^{\uparrow}_{TOA} - LW^{\uparrow}_{TOA} \tag{1}$$

$$SFC_{net} = SW^{\downarrow}_{SFC} - SW^{\uparrow}_{SFC} + LW^{\downarrow}_{SFC} - \sigma T_s^4 - SH_{SFC} - LH_{SFC} \tag{2}$$

$$F_{net} = TOA_{net} - SFC_{net} \tag{3}$$

In equations 1-3, SW, LW, SH, and LH indicate shortwave radiation, longwave radiation, sensible heat, and latent heat, respectively; T_s is the radiative surface temperature, and σ is the Stephan-

Boltzmann constant. The sign convention is such that a positive TOA_{net} represents energy gained by the atmosphere plus ocean/land, while a positive SFC_{net} represents energy gained by the surface. Positive values of equation F_{net} represent a gain of energy by the atmospheric column, either from the TOA or the surface.

A positive (negative) F_{net} value results in horizontal transport of energy out of (in to) the atmospheric column. The column energy source is positive in the tropics (where more energy is added to the atmospheric column through its top and bottom than is lost), and it is negative in the high latitudes (where more energy is lost from the top or bottom of the atmosphere than is gained), implying a transport of energy by the atmosphere from the equator to the poles (figure 6a). We define the energy flux equator (EFE) to be the latitude where the column-integrated poleward transport of energy is zero, which is generally located near the ITCZ (Kang et al. 2008; Bischoff and Schneider 2014; Adam et al. 2016). If the EFE is not centered on the equator, there is atmospheric energy transport across the equator. The relationship between the magnitude of cross-equatorial energy transport and the location of the ITCZ has been explored for the modern Earth system, where the ITCZ shifts 2.4-2.7°S per PW increase in northward cross-equatorial energy transport (Donohoe et al. 2013). In our idealized simulations, we find a similar relationship, with a 2.7° southward shift in the ITCZ per PW increase in northward cross-equatorial energy transport across all simulations and all seasons (4.0°S/PW if only annual mean values are considered) (figure S8, S9).

The cross-equatorial atmospheric energy transport is fuelled by the hemispheric asymmetry in F_{net} (Kang et al. 2008; Yoshimori and Broccoli 2008; Fasullo and Trenberth 2008; Donohoe et al. 2013). Transport of energy from the tropics to the mid-latitudes and between the hemispheres occurs via the Hadley circulation (Hadley 1735; Pierrehumbert 2002). The ITCZ is centered on the upwelling branch of the Hadley circulation (Dima and Wallace 2003; Bischoff and Schneider 2014). Note that changes in the strength of the Hadley circulation do not necessarily equate to

changes in atmospheric energy transport, as changes in the gross moist stability of the atmosphere can modify the amount of energy the Hadley circulation transports per unit mass transport (Neelin and Held 1987; Frierson 2007). Therefore, we first examine changes in the strength of the Hadley circulation (the maximum in the zonal mean streamfunction), then explore changes in the ITCZ in relation to the EFE in section *d*.

In our NorthlandBright simulation, the lower albedo of the southern (ocean) hemisphere means that the SH absorbs more energy than the NH (figure 6a). The strength of the Hadley cell is about twice as strong in DJF than in JJA in the NorthlandBright simulation (figure 6b-e). The Hadley cell is weaker in JJA than in DJF in part because the albedo of the NH is higher than that of the ocean hemisphere, and because the energy imbalance between the northern and southern hemispheres is smaller during JJA than DJF. This is because the ocean absorbs a large amount of energy during SH summer, which is then released to the atmosphere during NH summer. In contrast, the land stores very little energy, so during SH summer, the energy imbalance between the SH and NH is large both because of the lower SH albedo and because the surface heat source to the atmosphere in the NH is small (figure 7a-c).

(II) Circulation response to land albedo

Decreasing the albedo of the land surface so that it is the same as that of the ocean (Northland-Dark) results in more energy absorbed in the NH during NH summer, such that the northern and southern hemispheres absorb a similar amount of energy at the TOA (figure 6a, blue lines). In response to this reduction of the hemispheric energy imbalance, the Hadley circulation shifts towards the energy-rich NH. During JJA, the Hadley cell and the ITCZ both intensify, while during DJF, the Hadley cell weakens (figure 6b,c).

(III) CIRCULATION RESPONSE TO LAND EVAPORATION

The Hadley cell in DJF is stronger in NorthlandDry than in NorthlandBright (figure 6d). The reduced atmospheric water vapor from suppressed land evaporation (which causes the low land surface temperatures in NorthlandDry) results in less energy absorption by the NH atmosphere (figure 7h,i). So, even without direct modification of the surface in the SH, the SH in NorthlandDry is energy-rich compared to the NH. During JJA, the Hadley cell that is present in NorthlandBright collapses; instead there are two overturning circulations stacked on the equator; the lower cell circulates anti-clockwise while the upper cell circulates clockwise (figure 6e, S10).

d. Land influence on ITCZ location

In general, theory suggests that as the hemispheric energy imbalance increases, the ITCZ and EFE shift increasingly poleward into the energetically rich hemisphere (see discussion and references in Geen et al. 2020). With the exception of JJA in the NorthlandDry simulation (which does not feature a Hadley Cell - see figure S10), this behaviour is evident in all seasons in all of the Northland experiments (figure S8, S9).

Here, we explore two interesting results: the latitudinal extrema in ITCZ location in all of the Northland simulations is much farther polewards in *both* hemispheres than the ITCZ in the aquaplanet simulation (Aqua); in NorthlandBright, the ITCZ extends farther poleward into the ocean hemisphere than into the land hemisphere, despite the NH having a smaller heat capacity (figure 1b). This is surprising because past studies – in aquaplanet simulations – have shown that a shallower slab ocean allows for the ITCZ to extend farther polewards compared to a deep ocean (Bordoni and Schneider 2008; Wei and Bordoni 2018). The heat capacity of our continent is comparable to that of a 2m mixed layer ocean. However, water availability limits the poleward displacement of ITCZ over the continent.

(I) POLEWARD ITCZ EXTENT IN NORTHLANDDARK VS AQUA DURING JJA

NorthlandDark and Aqua both have a surface albedo of $\alpha = 0.25$ everywhere, thus, we focus on the ITCZ differences in these two experiments. The primary differences between NorthlandDark and Aqua are (i) NorthlandDark's limited capacity to hold water in the northern (land) hemisphere and (ii) a smaller heat capacity in the northern (land) hemisphere of NorthlandDark. With all else held equal, the NH would absorb the same amount of solar radiation as the SH. However, because there is less atmospheric water vapor over most of the NH in NorthlandDark than in Aqua, less SW energy is absorbed in JJA while more SW is absorbed in DJF (figures S11, S12, S13). Hence, if the ITCZ location were simply a function of an imbalance in absorbed solar radiation, we would expect the ITCZ of Aqua to be more polewards than the ITCZ of NorthlandDark during NH summer, which is not the case (figure 5). To understand why the ITCZ of NorthlandDark (and NorthlandBright and NorthlandDry) extends so much farther polewards than the ITCZ of Aqua, we must consider the seasonal storage and release of energy by the ocean, and differences in the atmospheric absorption of longwave radiation between hemispheres and simulations.

In Aqua, there is a net influx of energy at the TOA over the SH during DJF due to high insolation (figure 7, table S2). Some of this energy is absorbed by the ocean, but the net source of energy to the atmosphere is still positive. The NH atmosphere loses energy during DJF out the TOA (blue lines in figure 7). However, the NH ocean releases energy to the atmosphere at the surface (green lines in figure 7), though not enough to compensate for the loss of energy at the TOA, so the net source of energy to the atmosphere is negative over the NH during DJF. Thus, Aqua has an imbalance in atmospheric energy between the SH and NH (black lines in figure 7, table S2). The hemispheric energy imbalance of the atmosphere is damped by the surface (a) taking up energy from the atmosphere in the summer hemisphere and (b) releasing energy to the atmosphere in the

winter hemisphere. The damped hemispheric energy imbalance stems from the high heat capacity of the ocean; by increasing the heat capacity, the inter-hemispheric difference in atmospheric energy absorption is muted, and hence the poleward extent of the ITCZ is muted in both summer and winter in Aqua compared to NorthlandDark.

NorthlandDark has a larger hemispheric energy imbalance ΔF_{net} than Aqua during DJF, and the EFE sits much further south (31°S in NorthlandDark, vs 17°S in Aqua; table S2). As the latitude of the EFE and ITCZ are highly correlated in our simulations (figures S8, S9), this results in the ITCZ extending farther poleward in DJF.

(II) Poleward ITCZ extent in NorthlandDark vs Aqua in DJF

The energy balance of the SH in Aqua is very similar to that in NorthlandDark (figures 7, S14). This is expected because both worlds feature an ocean in the SH with the same albedo. Hence, the ITCZ in DJF is farther poleward in NorthlandDark than in Aqua because of differences in the atmospheric energy balance of the land hemisphere.

During DJF in the NorthlandDark simulation, there is a net flux of energy into the SH atmosphere, with energy being absorbed by the ocean, just like in Aqua (figure 7). However, in the NH, the energy released from the land surface to the atmosphere is much smaller in NorthlandDark than in Aqua, due to the smaller heat capacity of the land surface compared to the 20m deep mixed layer ocean (green lines, figure 7e,k). In addition, the lower atmospheric water vapor concentrations over the continent compared to the ocean means that less of the energy emitted by the land surface is actually absorbed by the atmosphere (blue lines, figure 7e,k). Thus, while the SH in Aqua and Northland Dark has comparable net energy input to the atmosphere during DJF, the NH in NorthlandDark has a greater energy deficit compared to the NH in Aqua (black lines, figure 7e,k; table S2). Based on the energy balance argument, we would expect this to lead to a south-

wards shift of the DJF ITCZ - that is, the DJF ITCZ is pushed farther away from the continent in NorthlandDark compared to Aqua. This is in fact true, as discussed above (figure 5).

(III) The polewards extent of the ITCZ in NorthlandBright and NorthlandDry

As argued in the previous two subsections, when we consider storage and release of energy from the land and ocean surface, as well as the absorption of longwave radiation by atmospheric water vapor, the imbalance of energy between the hemispheres is consistent with an ITCZ which extends farther polewards in NorthlandDark compared to Aqua. These arguments also apply to the ITCZ location in both NorthlandBright and NorthlandDry. NorthlandBright has the additional effect of a higher NH albedo, and as such, there is a smaller source of energy to the atmosphere during JJA compared to NorthlandDark (figure 7a-c and 2). Thus, the NH JJA ITCZ is weaker in NorthlandBright than NorthlandDark; however, it is still farther polewards than the ITCZ in Aqua. In the case of NorthlandDry (figure 7g-i), the reduced NH water vapor greatly reduces the energy source to the atmosphere during JJA in the NH (indeed, the energy source to the atmosphere during JJA is near zero, and is negative during DJF). Thus, independent of the lack of water to support an ITCZ over the continent in NorthlandDry, the energetic argument alone would suggest that the JJA ITCZ should be much weaker in NorthlandDry than in NorthlandDark. As in NorthlandDark, the SH energy budget in DJF is similar to that in Aqua for both NorthlandBright and NorthlandDry. Thus, as was the case for NorthlandDark, the poleward shift in the ITCZ for NorthlandDry and NorthlandBright is due to differences in the NH energy budget (specifically, the lack of a surface heat source).

4. Discussion

With all else held equal, reducing evaporation from the land surface should lead to surface warming, as the energy formerly used to evaporate water is instead re-partitioned into sensible heat or emitted longwave radiation. While reducing evaporation from the land surface directly leads to warming (Shukla and Mintz 1982; Laguë et al. 2019), reducing water flux from the land surface also impacts atmospheric concentrations of water vapor, a strong greenhouse gas.

Given the competing effects of reduced evaporative cooling which would lead to warming, and reduced longwave trapping by atmospheric water vapor which would lead to cooling, we hypothesize that a crossing-point exists in the temperature response to suppressed land evaporation (figure 8). Starting from a state of sufficient atmospheric moisture, reducing evaporation from the land surface initially leads to surface warming as a result of decreased evaporative cooling of the land surface ((i) in figure 8). However, as atmospheric water vapor concentration decreases, the strength of the atmospheric greenhouse effect also decreases, inducing a cooling effect on the surface; the warming signal from suppressed evaporation competes with the cooling from a reduced greenhouse effect ((ii) in figure 8). Once atmospheric concentrations of water vapor are sufficiently low, the cooling effect from the reduced atmospheric greenhouse effect dominates the surface temperature response ((iii) in figure 8).

In our NorthlandDry simulations, we find that suppressing terrestrial evaporation leads to cooling as a result of reduced atmospheric water vapor. We suspect our results differ from those of Shukla and Mintz (1982) and Laguë et al. (2019), who found that reduced evaporation leads to surface warming, primarily as a result of the continental configurations used in each study. Both Shukla and Mintz (1982) and Laguë et al. (2019) use a realistic, present-day Earth continental configuration. Thus, even if evaporation from land were completely suppressed, once air is advected

off the continents over the ocean, the atmospheric demand for moisture will lead to evaporation from the ocean, resulting in an increase in atmospheric water vapor content. Because there is ocean at all latitudes in the NH on present-day Earth, suppressed land evaporation does not lead to a large depletion of atmospheric water vapor. In contrast, NorthlandDry can only source atmospheric water vapor from the SH ocean, leading to a substantially drier atmosphere over the entire NH. While the atmospheric circulation brings some moisture onto the southern edge of the continent in the form of summertime precipitation, for the rest of the year the atmosphere has no source of water in the NH. This raises the question of how past continental configurations and distributions of water and vegetation on those continents may have impacted both terrestrial and global paleoclimate through water vapor feedbacks.

What is the distribution of continents that is required such that decreasing evapotranspiration from the land surface leads to a cooling rather than warming? In present-day Earth, the greenhouse effect is due mainly to water vapor, and the source of water vapor is net evaporation in the tropics (equatorward of 35° latitude) which is distributed globally by atmospheric circulation. In our Northland experiments, the continent covers the entire hemisphere, which severely reduces the evapotranspiration of water vapor poleward of the ITCZ in the NH. Hence, a further reduction of evapotranspiration in the NorthlandDry experiment reduces the greenhouse effect and causes cooling. In this regard, it is illuminating to consider the Snowball Earth events: times when Earth was almost entirely frozen for millions of years (Kirschvink 1992; Hoffman et al. 2017). These events occurred a handful of times in Earth's history, when most of the continental land masses were located in the tropics (see Kump et al. 2004; Worsley and Kidder 1991, and references therein). The most recent of these global glaciations occurred during the Permian period (252-299 Myr ago), when the land masses formed the megacontinent, Pangea (Shen et al. 2010). Prior to the glaciation, the proxy records suggest large swaths of the interior of Pangea were very dry (Parrish

1993). Future work could probe whether Pangea and other past tropical megacontinents were large enough to cause a sufficient reduction in tropical water vapor to cool the tropics, which would also cause even greater cooling in the extratropics as a consequence of reduced atmospheric energy transport (Rose et al. 2014). If so, cooling by reduced evapotranspiration would help explain why Snowball Earth happened.

In our Northland simulations, we find that the polewards extent of the ITCZ over the ocean hemisphere is influenced by the existence of the NH continent. Specifically, we find the small heat capacity and lower water vapor concentrations of the NH lead to the ocean hemisphere ITCZ extending much farther polewards than it does in an aquaplanet simulation. This is similar to the findings of Bordoni and Schneider (2008) and Wei and Bordoni (2018), that ITCZs in aquaplanets with shallower slab oceans extend farther polewards due to stronger energy gradients between the summer and winter hemisphers. Our Northland simulations also demonstrate the importance of hemispheric asymmetries in surface heat storage.

Previous studies have shown how hemispheric energy imbalances drive shifts in the zonal mean location of the ITCZ (e.g. Chiang and Bitz 2005; Broccoli et al. 2006; Kang et al. 2008; Swann et al. 2012). In the current continental configuration, zonal mean changes are not generally representative of regional precipitation change on Earth (Byrne and O'Gorman 2015; Kooperman et al. 2018; Atwood et al. 2020). However, given our meridionally symmetric continental distribution, the energy balance framework is a useful tool for understanding the seasonal cycle of circulation and the distribution of precipitation.

In Earth's present day continental configuration, roughly 68% of the total land mass is in the NH while the remaining 32% is in the SH. This work raises the question of how much the present day continental configuration impacts the ITCZ location via asymmetries in seasonal heat storage between the hemispheres. Past studies have explored how the continental distribution controls

where tropical SSTs peak (Philander et al. 1996), and in the present-day climate, asymmetries in hemispheric heat storage are further complicated by ocean heat uptake, which itself can impact ITCZ location (Frierson et al. 2013; Yu and Pritchard 2019).

Our Landworld and Lakeworld simulations, where there are no oceans, rapidly transport all the surface water to the poles. We expect this is because the climatological equator-to-pole temperature gradient ensures an even greater gradient in moisture (via the Clausius-Clapeyron relationship), and atmospheric storms transport water vapor towards the high latitudes where the vapor condenses and precipitates. The condensate remains at the poles because evaporation is greatly reduced by the cooling resulting from the reduced greenhouse effect. The continual reduction of atmospheric water vapor also explains why the Landworld and Lakeworld simulations cool over the 80 years of each simulation. During summer, some of the high-latitude soil moisture evaporates, but is locally recycled. In the absence of an efficient mechanism to transport moisture from the poles towards the equator, all the moisture ends up accumulating in the polar regions. This "leaking" of moisture from the tropics to the poles warrants further study: e.g. how much water does the system require to maintain a moist tropics? What controls the latitudinal extent of the polar lake? This distribution of surface water is similar to that on other planets, such as Mars, which has two polar ice caps (Boynton et al. 2002a; Wordsworth 2016; Feldman et al. 2004). While the mechanism by which the water on Mars is concentrated in its polar regions is unclear (Wordsworth 2016), we note that this is an intriguing similarity with our all-land simulations. The presence of large topographical features could potentially modify the distribution of water on a land planet, as it could favour the formation of lakes via runoff into basins rather than at the poles, where the distribution of the lakes would be controlled by surface topography rather than atmospheric moisture transport alone, as is the case in our simulations.

Certain caveats and limitations are inherent in our idealized framework. In this simplified GCM, there are no feedbacks associated with clouds. While cloud responses to terrestrial forcings have been identified in several studies (Hohenegger et al. 2009; de Arellano et al. 2012; Laguë and Swann 2016; Cho et al. 2018; Laguë et al. 2019; Kim et al. 2020), cloud responses are also a large source of uncertainty (Stocker et al. 2013; Zelinka et al. 2017). We have also ignored surface albedo feedbacks associated with changes in snow or ice; while our simulations can drop below freezing, that has no effect on the surface albedo. We would expect the addition of an albedo feedback to amplify cooling when temperatures drop below freezing.

5. Conclusions

In this study, we use an idealized climate model to study the climate of Northland, a planet with a continent covering the NH and an ocean covering the SH. The physical properties of the land surface differ from the ocean in several ways, each of which has an effect on the climate system. Land has a limited capacity to hold water, a higher albedo, and a smaller heat capacity than oceans, and evaporation and turbulent energy exchange from the land surface is influenced by properties of vegetation and soils. By conducting a series of simulations where specific properties of the land surface are modified, we test the sensitivity of surface climate and atmospheric circulation to various aspects of the land surface.

The climatology of Northland has a seasonal temperature cycle that is greatly amplified over the land hemisphere, due to the limited heat capacity of the land surface. On the continent, the tropics are seasonally wet; moisture is brought onto the continent from the ocean by the land-falling ITCZ, but the soils dry out during NH winter. From 20°N-40°N, there is a desert region. In the high latitudes, soils are moist year round. There is rain over high latitude land during NH summer; in contrast, precipitation declines polewards of 45°S in the ocean hemisphere in all seasons.

To further explore the accumulation of moisture over the northern high latitudes in Northland, we consider a land planet with no ocean, that is initialized with the same amount of water over every land gridcell. Within just a few simulation years, all of the water has accumulated over the polar regions, leaving the lower latitudes dry. This is similar to the distribution of water on Mars, where most moisture is locked in two polar ice caps (Boynton et al. 2002b; Wordsworth 2016; Feldman et al. 2004).

Decreasing the land albedo leads to warming, as we would expect from the corresponding increase in absorbed solar radiation. Surprisingly, we find that suppressing evaporation from the land surface leads to global-scale cooling, with particularly large cooling over the NH continent. With all else held equal, decreasing evaporation would lead to warming as the land surface would have to shed energy through sensible heat or emitted longwave radiation, both of which are a function of surface temperature. However, in our simulations, we find that suppressing terrestrial evaporation reduces atmospheric water vapor concentrations, and in turn decreases the strength of the greenhouse effect. The decrease in longwave radiation trapping by water vapor leads to surface cooling which outweighs any surface warming that may have resulted directly from reduced evaporative cooling. This behaviour suggests the existence of a threshold in the climate response to reduced terrestrial evaporation; below the threshold, reducing terrestrial evaporation leads to warming by directly reducing latent cooling of the surface, while above the threshold, the cooling effect of reduced longwave trapping by water vapor dominates the surface temperature response.

We find that the ITCZ extends much further polewards, both over the land and ocean hemispheres, in our Northland simulations compared to an aquaplanet simulation. This is the result of the difference in surface heat capacity and atmospheric water vapor between the land and ocean hemispheres, which leads to a larger hemispheric imbalance in atmospheric energy in the Northland simulations compared to an aquaplanet.

By exploring the climate of Northland, this study provides insight into the role of hemispheric asymmetries in continental distribution on surface climate and atmospheric circulation, as well as into energetic constraints on the ITCZ location. Northland provides an ideal limit for probing fundamental impacts of hemispheric asymmetries and raises new questions about the role of continental distribution, planetary albedo, and terrestrial evaporation in modulating the climate system.

Data availability statement. The Isca climate model is publicly available at `https://github.com/ExeClim/Isca`. The data presented in this paper will be archived on Dryad and the link added here upon acceptance of this manuscript.

Acknowledgments. We wish to thank the organizers of the 2018 Advanced Climate Dynamics Course, where this project began (https://www.uib.no/en/rs/acdc/118773/acdc-2018-hemispheric-asymmetry-climate). We thank W. R. Boos and A. L. S. Swann for their helpful discussions and feedback. We acknowledge postdoctoral funding support for MML from the James S. McDonnell Foundation. MP acknowledges funding by the University of Exeter College of Engineering Mathematics and Physical Sciences, and the UK - China Research and Innovation Partnership Fund through the Met Office Climate Science for Service Partnership (CSSP) China as part of the Newton Fund. In addition, MP's gratitude is due to the Rupert Ford Award (administered by the Royal Meteorological Society) and the University of Exeter College of Engineering Mathematics and Physical Sciences PhD Mobility Fund who provided the funding for her research visit to the University of Washington, Seattle, which facilitated collaboration on this project.

References

Adam, O., T. Bischoff, and T. Schneider, 2016: Seasonal and interannual variations of the energy flux equator and ITCZ. Part I: Zonally averaged ITCZ position. *Journal of Climate*, **29 (9)**, 7281–7293, doi:10.1175/JCLI-D-15-0710.1.

Atwood, A. R., A. Donohoe, D. S. Battisti, X. Liu, and F. S. R. Pausata, 2020: Robust longitudinally-variable responses of the ITCZ to a myriad of climate forcings. *ESSOAR Preprint. Submitted to GRL.*, **(May)**, 1–13, doi:https://doi.org/10.1002/essoar.10503115.1.

Bischoff, T., and T. Schneider, 2014: Energetic constraints on the position of the intertropical convergence zone. *Journal of Climate*, **27 (13)**, 4937–4951, doi:10.1175/JCLI-D-13-00650.1.

Bonan, G. B., 2008: Ecological Climatology. Cambridge Univ. Press, Cambridge, UK.

Bordoni, S., and T. Schneider, 2008: Monsoons as eddy-mediated regime transitions of the tropical overturning circulation. *Nature Geoscience*, **1 (8)**, 515–519, doi:10.1038/ngeo248.

Boynton, W. V., and Coauthors, 2002a: Distribution of hydrogen in the near surface of Mars: Evidence for subsurface ice deposits. *Science*, **297 (5578)**, 81–85, doi:10.1126/science.1073722.

Boynton, W. V., and Coauthors, 2002b: Distribution of hydrogen in the near surface of mars: Evidence for subsurface ice deposits. *science*, **297 (5578)**, 81–85.

Broccoli, A. J., K. a. Dahl, and R. J. Stouffer, 2006: Response of the ITCZ to Northern Hemisphere cooling. *Geophysical Research Letters*, **33 (1)**, 1–4, doi:10.1029/2005GL024546.

Budyko, M. I., 1961: The Heat Balance of the Earth's Surface. *Soviet Geography*, **2 (4)**, 3–13, doi:10.1080/00385417.1961.10770761.

Budyko, M. I., 1969: The effect of solar radiation variations on the climate of the Earth. *Tellus*, **21 (5)**, 611–619, doi:10.3402/tellusa.v21i5.10109.

Byrne, M. P., and P. A. O'Gorman, 2015: The response of precipitation minus evapotranspiration to climate warming: Why the "Wet-get-wetter, dry-get-drier" scaling does not hold over land. *Journal of Climate*, **28 (20)**, 8078–8092, doi:10.1175/JCLI-D-15-0369.1.

Canadell, A. J., R. B. Jackson, J. R. Ehleringer, H. A. Mooney, O. E. Sala, and E. Schulze, 1996: Maximum Rooting Depth of Vegetation Types at the Global Scale. *Oecologia*, **108 (4)**, 583–595.

Cess, R. D., and S. D. Goldenberg, 1981: The effect of ocean heat capacity upon global warming due to increasing atmospheric carbon dioxide. *Journal of Geophysical Research*, **86 (80)**, 498–502.

Charney, J. G., 1975: Dynamics of deserts and drought in the Sahel. *Quarterly Journal of the Royal Meteorological Society*, **101 (428)**, 193–202, doi:10.1002/qj.49710142802, URL http://dx.doi.org/10.1002/qj.49710142802%5Cnpapers2://publication/doi/10.1002/qj.49710142802.

Cheng, L., K. E. Trenberth, J. Fasullo, T. Boyer, J. Abraham, and J. Zhu, 2017: Improved estimates of ocean heat content from 1960 to 2015. *Science Advances*, **3 (3)**, e1601 545.

Chiang, J. C. H., and C. M. Bitz, 2005: Influence of high latitude ice cover on the marine Intertropical Convergence Zone. *Climate Dynamics*, **25 (5)**, 477–496, doi:10.1007/s00382-005-0040-5.

Cho, M. H., A. R. Yang, E. H. Baek, S. M. Kang, S. J. Jeong, J. Y. Kim, and B. M. Kim, 2018: Vegetation-cloud feedbacks to future vegetation changes in the Arctic regions. *Climate Dynamics*, **50 (9-10)**, 3745–3755, doi:10.1007/s00382-017-3840-5.

Croll, J., 1870: XII. On ocean-currents. *The London, Edinburgh, and Dublin Philosophical Magazine and Journal of Science*, **39 (259)**, 81–106.

Davin, E. L., N. de Noblet-Ducoudré, N. de Noblet-Ducoudre, and N. de Noblet-Ducoudré, 2010: Climatic Impact of Global-Scale Deforestation: Radiative versus Nonradiative Processes. *Journal of Climate*, **23 (1)**, 97–112, doi:10.1175/2009JCLI3102.1, URL http://journals.ametsoc.org/doi/abs/10.1175/2009JCLI3102.1.

de Arellano, J. V.-G., C. C. van Heerwaarden, and J. Lelieveld, 2012: Modelled suppression of boundary-layer clouds by plants in a CO2-rich atmosphere. *Nature Geoscience*, **5 (10)**, 701–704, doi:10.1038/ngeo1554, URL http://dx.doi.org/10.1038/ngeo1554.

Dima, I. M., and J. M. Wallace, 2003: On the seasonality of the Hadley Cell. *Journal of the Atmospheric Sciences*, **60 (12)**, 1522–1527, doi:10.1175/1520-0469(2003)060⟨1522:OTSOTH⟩2.0.CO;2.

Donohoe, A., K. C. Armour, G. H. Roe, D. S. Battisti, and L. Hahn, 2020: The Partitioning of Meridional Heat Transport from the Last Glacial Maximum to CO 2 Quadrupling in Coupled Climate Models . *Journal of Climate*, **33 (10)**, 4141–4165, doi:10.1175/jcli-d-19-0797.1.

Donohoe, A., and D. S. Battisti, 2011: Atmospheric and surface contributions to planetary albedo. *Journal of Climate*, **24 (16)**, 4402–4418, doi:10.1175/2011JCLI3946.1.

Donohoe, A., J. Marshall, D. Ferreira, and D. Mcgee, 2013: The relationship between ITCZ location and cross-equatorial atmospheric heat transport: From the seasonal cycle to the last glacial maximum. *Journal of Climate*, **26 (11)**, 3597–3618, doi:10.1175/JCLI-D-12-00467.1.

Eliassen, A., and E. Palm, 1960: On the Transfer of Energy in Stationary Mountain Waves. *Geofysiske Publikasjoner*.

Fasullo, J. T., and K. E. Trenberth, 2008: The Annual Cycle of the Energy Budget. Part II: Meridional Structures and Poleward Transports. *Journal of Climate*, **21 (10)**, 2313–2325, doi: 10.1175/2007JCLI1936.1.

Feldman, W. C., and Coauthors, 2004: Global distribution of near-surface hydrogen on mars. *Journal of Geophysical Research: Planets*, **109 (E9)**.

Ferrari, R., and D. Ferreira, 2011: What processes drive the ocean heat transport? *Ocean Modelling*, **38 (3)**, 171–186, doi:10.1016/j.ocemod.2011.02.013, URL http://www.sciencedirect.com/science/article/pii/S1463500311000485.

Forget, G., and D. Ferreira, 2019: Global ocean heat transport dominated by heat export from the tropical Pacific. *Nature Geoscience*, 1, doi:10.1038/s41561-019-0333-7, URL http://www.nature.com/articles/s41561-019-0333-7.

Frierson, D. M., 2007: The dynamics of idealized convection schemes and their effect on the zonally averaged tropical circulation. *Journal of the Atmospheric Sciences*, **64 (6)**, 1959–1974, doi:10.1175/JAS3935.1.

Frierson, D. M. W., and Coauthors, 2013: Contribution of ocean overturning circulation to tropical rainfall peak in the Northern Hemisphere. *Nature Geoscience*, **6 (11)**, 940–944.

Geen, R., S. Bordoni, D. Battisti, and K. Hui, 2020: The Dynamics of the Global Monsoon - Connecting Theory and Observations. *Earth and Space Science Open Archive*, 1–26, doi:https://doi.org/10.1002/essoar.10502409.1.

Hadley, G., 1735: Concerning the Cause of the General Trade-Winds. *Royal Society of London Philosophical Transactions Series I*, **39**, 58–62.

Hartmann, D. L., 1994: *Global physical climatology*, Vol. 56. Academic press.

Held, I. M., 2005: The gap between simulation and understanding in climate modeling. *Bulletin of the American Meteorological Society*, **86 (11)**, 1609–1614.

Held, I. M., P. L. Panetta, and R. T. Pierrehumbert, 1985: Stationary external Rossby waves in vertical shear. 865–883 pp., doi:10.1175/1520-0469(1985)042⟨0865:SERWIV⟩2.0.CO;2.

Hoffman, P. F., and Coauthors, 2017: Snowball Earth climate dynamics and Cryogenian geology-geobiology. *Science Advances*, **3 (11)**, doi:10.1126/sciadv.1600983.

Hohenegger, C., P. Brockhaus, C. S. Bretherton, and C. Schär, 2009: The soil moisture-precipitation feedback in simulations with explicit and parameterized convection. *Journal of Climate*, **22 (19)**, 5003–5020, doi:10.1175/2009JCLI2604.1.

Jeevanjee, N., P. Hassanzadeh, S. Hill, and A. Sheshadri, 2017: A perspective on climate model hierarchies. *Journal of Advances in Modeling Earth Systems*, **9 (4)**, 1760–1771, doi:10.1002/2017MS001038.

Jin, Z., T. P. Charlock, W. L. Smith, and K. Rutledge, 2004: A parameterization of ocean surface albedo. *Geophysical Research Letters*, **31 (22)**, 1–4, doi:10.1029/2004GL021180.

Kang, S. M., 2020: Extratropical Influence on the Tropical Rainfall Distribution. **1**, 24–36.

Kang, S. M., I. M. Held, D. M. W. Frierson, and M. Zhao, 2008: The Response of the ITCZ to Extratropical Thermal Forcing: Idealized Slab-Ocean Experiments with a GCM. *Journal of Climate*, **21 (14)**, 3521–3532, doi:10.1175/2007JCLI2146.1.

Kang, S. M., R. Seager, D. M. W. Frierson, and X. Liu, 2015: Croll revisited: Why is the Northern Hemisphere warmer than the Southern Hemisphere? *Climate Dynamics*, **44 (5-6)**, 1457–1472.

Kim, J. E., M. M. Laguë, and A. L. S. Swann, 2020: Evaporative Resistance is of Equal Importance as Surface Albedo in High-Latitude Surface Temperatures Due to Cloud Feedbacks. 1–10, doi: 10.1029/2019GL085663.

Kirschvink, J. L., 1992: Late Proterozoic low-latitude global glaciation: the snowball Earth. *The Proterozoic Biosphere*, **52**, 51–52, doi:10.1038/scientificamerican0100-68.

Kooperman, G. J., Y. Chen, F. M. Hoffman, C. D. Koven, K. Lindsay, M. S. Pritchard, A. L. S. Swann, and J. T. Randerson, 2018: Forest response to rising CO2 drives zonally asymmetric rainfall change over tropical land. *Nature Climate Change*, **8**, doi: 10.1038/s41558-018-0144-7.

Kuhlbrodt, T., and J. Gregory, 2012: Ocean heat uptake and its consequences for the magnitude of sea level rise and climate change. *Geophysical Research Letters*, **39 (18)**.

Kump, L. R., J. F. Kasting, R. G. Crane, and others, 2004: *The Earth System*, Vol. 432. Pearson Prentice Hall Upper Saddle River, NJ.

Laguë, M. M., G. B. Bonan, and A. L. S. Swann, 2019: Separating the Impact of Individual Land Surface Properties on the Terrestrial Surface Energy Budget in both the Coupled and Uncoupled Land–Atmosphere System. *Journal of Climate*, **32 (18)**, 5725–5744, doi:10.1175/jcli-d-18-0812.1.

Laguë, M. M., and A. L. S. Swann, 2016: Progressive Mid-latitude Afforestation: Impacts on Clouds, Global Energy Transport, and Precipitation. *Journal of Climate*, **29 (15)**, 5561–5573, doi:10.1175/JCLI-D-15-0748.1, URL http://dx.doi.org/10.1175/JCLI-D-15-0748.1.

Levins, R., 1966: The Strategy of Model Building in Polulation Biology. *American Scientist*, **5 (41)**, 420–431.

Lindzen, R. S., M.-D. Chou, and A. Y. Hou, 2001: Does the earth have an adaptive infrared iris? *Bulletin of the American Meteorological Society*, **82 (3)**, 417–432.

Loft, G., 1918: The Gulf Stream and the North Atlantic Drift. *Journal of Geography*, **17 (1)**, 8–17, doi:10.1080/00221341808984367.

Maher, P., and Coauthors, 2019: Model Hierarchies for Understanding Atmospheric Circulation. doi:10.1029/2018RG000607.

Manabe, S., 1969: Climate and the Ocean Circulation 1. *Monthly Weather Review*, **97 (11)**, 739–774, doi:10.1175/1520-0493(1969)097⟨0739:CATOC⟩2.3.CO;2, URL http://journals.ametsoc.org/doi/abs/10.1175/1520-0493(1969)097%3C0739:CATOC%3E2.3.CO;2.

Manabe, S., R. J. Stouffer, M. J. Spelman, and K. Bryan, 1991: Transient responses of a coupled ocean–atmosphere model to gradual changes of atmospheric CO2. Part I. Annual mean response. *Journal of Climate*, **4 (8)**, 785–818.

Manabe, S., and T. B. Terpstra, 1974: The effect of moutains on the general circulation of the Atmosphere. 3 pp.

Marshall, D. P., and L. Zanna, 2014: A conceptual model of ocean heat uptake under climate change. *Journal of Climate*, **27 (22)**, 8444–8465.

Marshall, J., and R. A. Plumb, 2008: *Atmosphere, ocean, and climate dynamics: an introductory text*, Vol. 93. Elsevier Academic Press.

McFarlane, N. A., 1987: The Effect of Orographically Excited Gravity Wave Drag on the General Circulation of the Lower Stratosphere and Troposphere. 1775–1800 pp., doi:10.1175/1520-0469(1987)044⟨1775:teooeg⟩2.0.co;2.

McMullin, E., 1985: Galilean idealization. *Studies in History and Philosophy of Science Part A*, **16 (3)**, 247–273.

Milly, P. C. D., and a. B. Shmakin, 2002: Global Modeling of Land Water and Energy Balances. Part I: The Land Dynamics (LaD) Model. *Journal of Hydrometeorology*, **3 (3)**, 283–299, doi:10.1175/1525-7541(2002)003⟨0283:GMOLWA⟩2.0.CO;2, URL http://journals.ametsoc.org/doi/abs/10.1175/1525-7541%282002%29003%3C0283%3AGMOLWA%3E2.0.CO%3B2.

Neelin, J. D., and I. M. Held, 1987: Modeling tropical convergence based on the moist static energy budget. 3–12 pp., doi:10.1175/1520-0493(1987)115⟨0003:MTCBOT⟩2.0.CO;2.

North, G. R., J. G. Mengel, and D. A. Short, 1983: Simple energy balance model resolving the seasons and the continents: application to the astronomical theory of the ice ages. *Journal of Geophysical Research*, **88 (C11)**, 6576–6586, doi:10.1029/JC088iC11p06576.

Oke, T. R., 1987: *Boundary layer climates, Second edition*. doi:10.1017/CBO9781107415324.004.

Parrish, J. T., 1993: Climate of the supercontinent Pangea. *The Journal of Geology*, **101 (2)**, 215–233.

Payne, R. E., 1972: Albedo of the Sea Surface. 959–970 pp., doi:10.1175/1520-0469(1972)029⟨0959:aotss⟩2.0.co;2.

Philander, S. G. H., and Coauthors, 1996: Why the ITCZ is mostly north of the equator. *Journal of climate*, **9 (12)**, 2958–2972, doi:10.1175/1520-0442(1996)009⟨2958:WTIIMN⟩2.0.CO;2.

Pierrehumbert, R. T., 2002: The hydrologic cycle in deep-time climate problems. *Nature*, **419 (6903)**, 191–198, doi:10.1038/nature01088.

819 Queney, P., 1948: The Problem of Air Flow Over Mountains: A Summary of Theoretical Studies.
820 *Bulletin of the American Meteorological Society*, **29 (1)**, 16–26, doi:10.1175/1520-0477-29.1.
821 16.

822 Richardson, P. L., 1980: Benjamin Franklin and Timothy Folger's First Printed Chart of the Gulf
823 Stream. *Science*, **207 (4431)**, 643–645.

824 Rose, B. E. J., K. C. Armour, D. S. Battisti, N. Feldl, and D. D. B. Koll, 2014: The dependence of
825 transient climate sensitivity and radiative feedbacks on the spatial pattern of ocean heat uptake.
826 *Geophysical Research Letters*, **41 (3)**, 1071–1078.

827 Roychowdhury, R., and R. DeConto, 2019: Interhemispheric effect of global geography on Earth's
828 climate response to orbital forcing. *Climate of the Past*, **15 (1)**, 377–388.

829 Sellers, P. J., and Coauthors, 1996: Comparison of radiative and physiological effects of dou-
830 bled atmospheric CO2 on climate. *SCIENCE-NEW YORK THEN WASHINGTON-*, **271 (5254)**,
831 1402–1405, doi:10.1126/science.271.5254.1402.

832 Sellers, W. D., 1969: Global Climatic Model Based on the Energy Balance of the Earth- Atmo-
833 sphere System. *Journal of Applied Meteorology*, **8 (3)**, 392–400.

834 Shen, S. Z., M. Y. Zhu, X. D. Wang, G. X. Li, C. Q. Cao, and H. Zhang, 2010: A comparison of
835 the biological, geological events and environmental backgrounds between the Neoproterozoic-
836 Cambrian and Permian-Triassic transitions. *Science China Earth Sciences*, **53 (12)**, 1873–1884,
837 doi:10.1007/s11430-010-4092-y.

838 Shukla, J., and Y. Mintz, 1982: Influence of Land-Surface Evapotranspiration on the Earth's Cli-
839 mate. *Science*, **215 (4539)**, 1498–1501.

Sikma, M., and J. Vilà-Guerau de Arellano, 2019: Substantial Reductions in Cloud Cover and Moisture Transport by Dynamic Plant Responses. *Geophysical Research Letters*, **46 (3)**, 1870–1878, doi:10.1029/2018GL081236.

Stephens, G. L., and Coauthors, 2008: CloudSat mission: Performance and early science after the first year of operation. *Journal of Geophysical Research: Atmospheres*, **113 (D8)**.

Stocker, T. F., and Coauthors, 2013: Climate change 2013 the physical science basis: Working Group I contribution to the fifth assessment report of the Intergovernmental Panel on Climate Change. *Contribution of Working Group I to the Fifth Assessment Report of the Intergovernmental Panel on Climate Change.*, **9781107057**, 1–1535, doi:10.1017/CBO9781107415324.

Stouffer, R. J., S. Manabe, and K. Bryan, 1989: Interhemispheric asymmetry in climate response to a gradual increase of atmospheric CO2. *Nature*, **342 (6250)**, 660–662.

Sud, Y. C., J. Shukla, and Y. Mintz, 1988: Influence of Land Surface Roughness on Atmospheric Circulation and Precipitation: A Sensitivity Study with a General Circulation Model. 1036–1054 pp., doi:10.1175/1520-0450(1988)027⟨1036:iolsro⟩2.0.co;2.

Sutton, R. T., B. Dong, and J. M. Gregory, 2007: Land/sea warming ratio in response to climate change: IPCC AR4 model results and comparison with observations. *Geophysical Research Letters*, **34 (2)**, 2–6, doi:10.1029/2006GL028164.

Swann, A. L. S., I. Y. Fung, and J. C. H. Chiang, 2012: Mid-latitude afforestation shifts general circulation and tropical precipitation. *Proceedings of the National Academy of Sciences*, **109 (3)**, 712–716, doi:10.1073/pnas.1116706108.

Trenberth, K. E., and J. M. Caron, 2001: Estimates of meridional atmosphere and ocean heat transports. *Journal of Climate*, **14 (16)**, 3433–3443.

Trenberth, K. E., and J. T. Fasullo, 2009: Global warming due to increasing absorbed solar radiation. *Geophysical Research Letters*, **36 (7)**.

Vallis, G. K., and Coauthors, 2018: Isca, v1.0: A framework for the global modelling of the atmospheres of Earth and other planets at varying levels of complexity. *Geoscientific Model Development*, **11 (3)**, 843–859, doi:10.5194/gmd-11-843-2018.

Wallace, J. M., Y. Zhang, and J. A. Renwick, 1995: Dynamic Contribution to Hemispheric Mean Temperature Trends. *Science*, **270 (5237)**, 780–783.

Wei, H.-H., and S. Bordoni, 2018: Energetic Constraints on the ITCZ Position in Idealized Simulations With a Seasonal Cycle. *Journal of Advances in Modeling Earth Systems*, **10 (7)**, 1708–1725, doi: 10.1029/2018MS001313.

Wiscombe, W., and S. Warren, 1980: A Model for Spectral Albedo I: Pure Snow. 2712–2733 pp.

Wordsworth, R. D., 2016: The Climate of Early Mars. *Annual Review of Earth and Planetary Sciences*, **44 (1)**, 381–408, doi:10.1146/annurev-earth-060115-012355.

Worsley, T. R., and D. L. Kidder, 1991: First-order coupling of paleogeography and CO 2 , with global surface temperature and its latitudinal contrast. *Geology*, **19 (12)**, 1161–1164, doi:10.1130/0091-7613(1991)019⟨1161:FOCOPA⟩2.3.CO;2.

Yoshimori, M., and A. J. Broccoli, 2008: Equilibrium Response of an Atmosphere–Mixed Layer Ocean Model to Different Radiative Forcing Agents: Global and Zonal Mean Response. *Journal of Climate*, **21 (17)**, 4399–4423, doi:10.1175/2008JCLI2172.1, URL http://dx.doi.org/10.1175/2008JCLI2172.1.

Yu, S., and M. S. Pritchard, 2019: A strong role for the AMOC in partitioning global energy transport and shifting ITCZ position in response to latitudinally discrete solar forcing in CESM1.2. *Journal of Climate*, **32 (8)**, 2207–2226, doi:10.1175/JCLI-D-18-0360.1.

Zelinka, M. D., D. A. Randall, M. J. Webb, and S. A. Klein, 2017: Clearing clouds of uncertainty. *Nature Climate Change*, **7 (10)**, 674–678, doi:10.1038/nclimate3402.

LIST OF TABLES

Table 1. List of the idealized-continent Isca simulations used in this study, along with the land surface property values that differentiate each experiment from the others. 44

TABLE 1. List of the idealized-continent Isca simulations used in this study, along with the land surface property values that differentiate each experiment from the others.

Experiment name	**Description**	**Land albedo**	**Bucket depth [m H_20]**	**Initial water in bucket [m H_20]**
NorthlandBright	Northern Hemisphere continent with an albedo brighter than the ocean.	0.325	0.15	0.1
NorthlandDark	Northern Hemisphere continent with the same albedo as the ocean.	0.25	0.15	0.1
NorthlandEmpty	Like NorthlandBright, but initialized with no water on the land surface.	0.325	0.15	0
NorthlandDry	Like NorthlandBright, but with a very small capacity for the land to hold water.	0.325	0.00001	0
Landworld	Like NorthlandBright, but with the entire globe covered with a continent (no oceans).	0.325	0.15	0.1
Lakeworld	Like Landworld, but with water conservation. Lakes are formed if the water content of a gridcell exceeds capacity.	0.325	0.15	0.1
Aqua	Aquaplanet simulation with 20m mixed layer (no land)	–	–	–

LIST OF FIGURES

Fig. 1. Zonal mean temperature (a,c) and precipitation (b,d). The NorthlandBright simulation is shown in (a) & (b) (solid lines). The anomalies for NorthlandDark - NorthlandBright (dashed lines) and NorthlandDry - NorthlandBright (dash-dot lines) are shown in (c) & (d). Black lines indicate annual mean values, while blue (red) show values for DJF (JJA). Shading in a-d indicates $\pm$ 1 standard deviation. Panels (e,f) show the change in zonal mean specific humidity (shading) and temperature (contours) for (e) NorthlandDark-NorthlandBright and (f) NorthlandDry-NorthlandBright. Temperature contours are spaced at 1K. Only humidity values in (e,f) which differ significantly ($p < 0.05$ using a student's t-test) are shown. 46

Fig. 2. Change in net energy flux at the TOA (top row), surface (middle row), and their difference (bottom row), for NorthlandDark - NorthlandBright (left column) and NorthlandDry - NorthlandBright (right column). Net TOA energy flux is defined as positive down; red values indicate more energy *into* the *atmosphere*. Net surface energy flux is defined as positive down; red values indicate more energy into the *surface*. The difference (TOA-SFC) is the net change in energy into the atmosphere; purple means more energy into the atmosphere (either from the surface or TOA), while green means less energy into the atmosphere. . . . 47

Fig. 3. Seasonal cycle of the change in zonal mean surface energy budget terms for NorthlandDark - NorthlandBright (a-e) and NorthlandDry - NorthlandBright (f-j). Change in net surface shortwave radiation (a,f), downwards longwave radiation (b,g), upwards longwave radiation (c,h), sensible heat flux (d,i), and latent heat flux (e,j). 48

Fig. 4. Zonal mean seasonal cycle of (a) precipitation, (b) evaporation, and (c) precipitation-evaporation (P-E) for the spun-up NorthlandBright simulation. Zonal mean terrestrial water storage over the first 6 simulation years for (d) NorthlandBright and (e) NorthlandEmpty. Zonal mean terrestrial water storage for the full 80 year simulations of (f) Landworld and (g) Lakeworld (note the non-linear colour bar). Cyan contour in (f,g) at 150mm shows the bucket capacity (i.e. fully saturated soil moisture). 49

Fig. 5. Seasonal cycle of zonal mean precipitation from 40°S to 40°N in (a) NorthlandBright, (b) NorthlandDark, (c) NorthlandDry, and (d) Aqua. 50

Fig. 6. (a) Zonal mean column energy source F_{net} for NorthlandBright (black), NorthlandDark (green), and NorthlandDry (brown) for the annual (black), JJA (red), and DJF (blue) mean. Contours in (b)-(e) show the NorthlandBright meridional stream function for DJF (b,d) and JJA (c,e), with shading showing the difference in the streamfunction between NorthlandDark-NorthlandBright (b,c) and NorthlandDry-NorthlandBright (d,e). Contour lines in b-d are spaced at 60×10^9 kg/s. The blue lines in (b)-(e) show the change in zonal mean precipitation. Panels (b,d) show DJF differences, while panels (c,e) show JJA differences. In panels (b-d), only values which differ significantly ($p < 0.05$ in a student's t-test) are shown. 51

Fig. 7. Zonally averaged net TOA energy flux (blue dotted line), net surface energy flux (green dash-dot line), and the atmospheric column energy source (TOA-SFC; black solid line) for the annual mean (top row), DJF (middle row) and JJA (bottom row). NorthlandBright is shown in the first column, NorthlandDark in the second, NorthlandDry in the third, and Aqua in the fourth. 52

Fig. 8. Schematic showing the possible surface temperature response to decreased terrestrial evaporation. 53

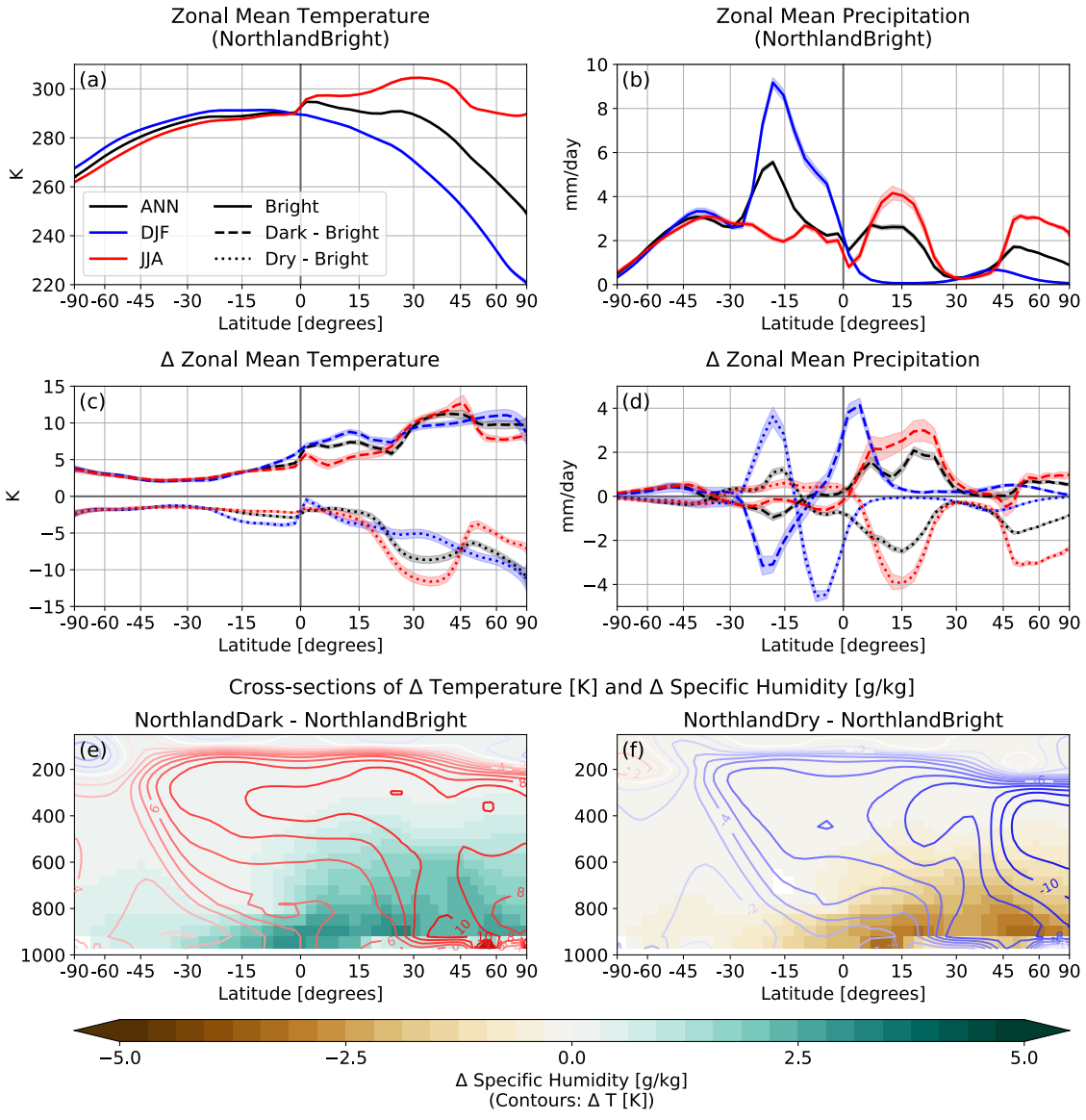

938 FIG. 1. Zonal mean temperature (a,c) and precipitation (b,d). The NorthlandBright simulation is shown in
939 (a) & (b) (solid lines). The anomalies for NorthlandDark - NorthlandBright (dashed lines) and NorthlandDry -
940 NorthlandBright (dash-dot lines) are shown in (c) & (d). Black lines indicate annual mean values, while blue
941 (red) show values for DJF (JJA). Shading in a-d indicates $\pm$ 1 standard deviation. Panels (e,f) show the change
942 in zonal mean specific humidity (shading) and temperature (contours) for (e) NorthlandDark-NorthlandBright
943 and (f) NorthlandDry-NorthlandBright. Temperature contours are spaced at 1K. Only humidity values in (e,f)
944 which differ significantly ($p < 0.05$ using a student's t-test) are shown.

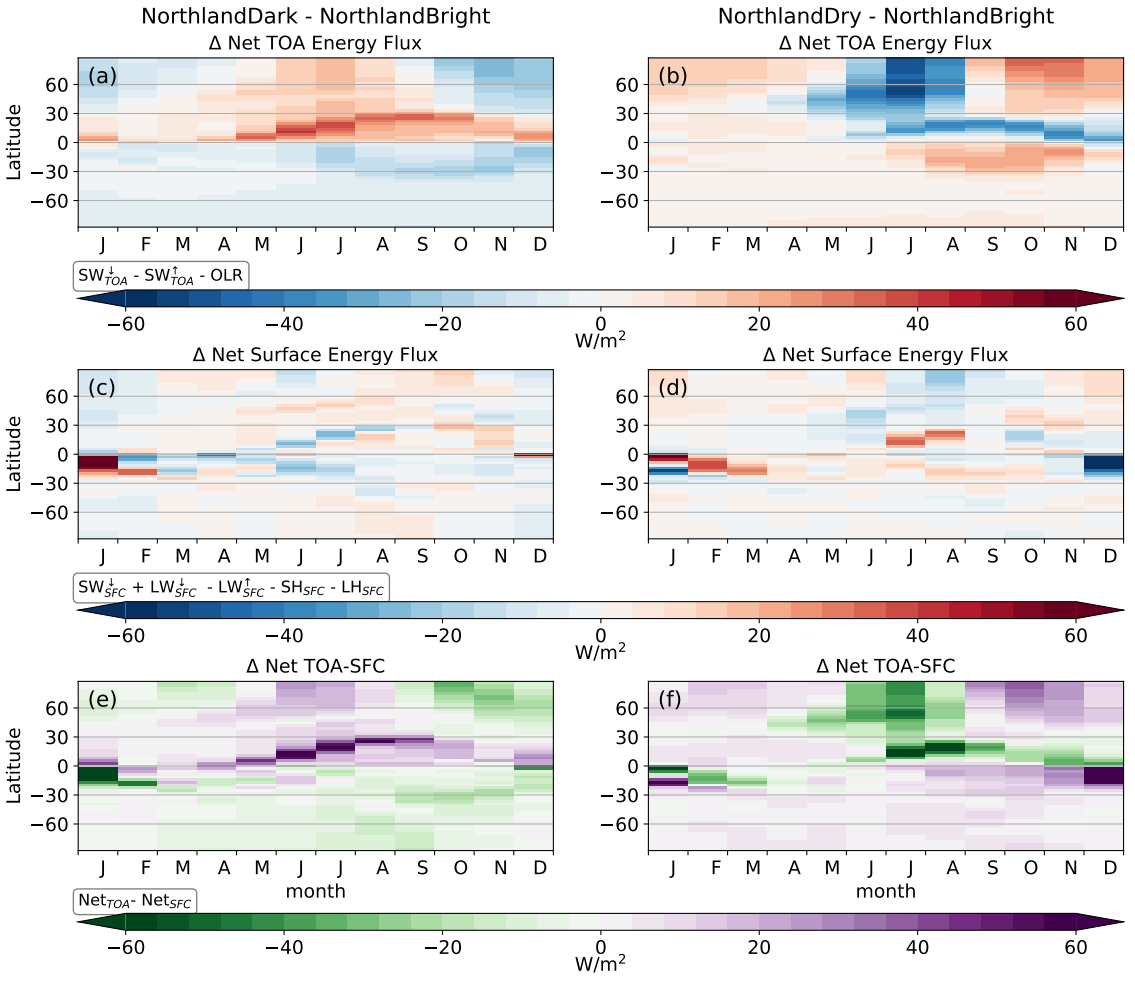

945 FIG. 2. Change in net energy flux at the TOA (top row), surface (middle row), and their difference (bottom
946 row), for NorthlandDark - NorthlandBright (left column) and NorthlandDry - NorthlandBright (right column).
947 Net TOA energy flux is defined as positive down; red values indicate more energy *into* the *atmosphere*. Net
948 surface energy flux is defined as positive down; red values indicate more energy into the *surface*. The difference
949 (TOA-SFC) is the net change in energy into the atmosphere; purple means more energy into the atmosphere
950 (either from the surface or TOA), while green means less energy into the atmosphere.

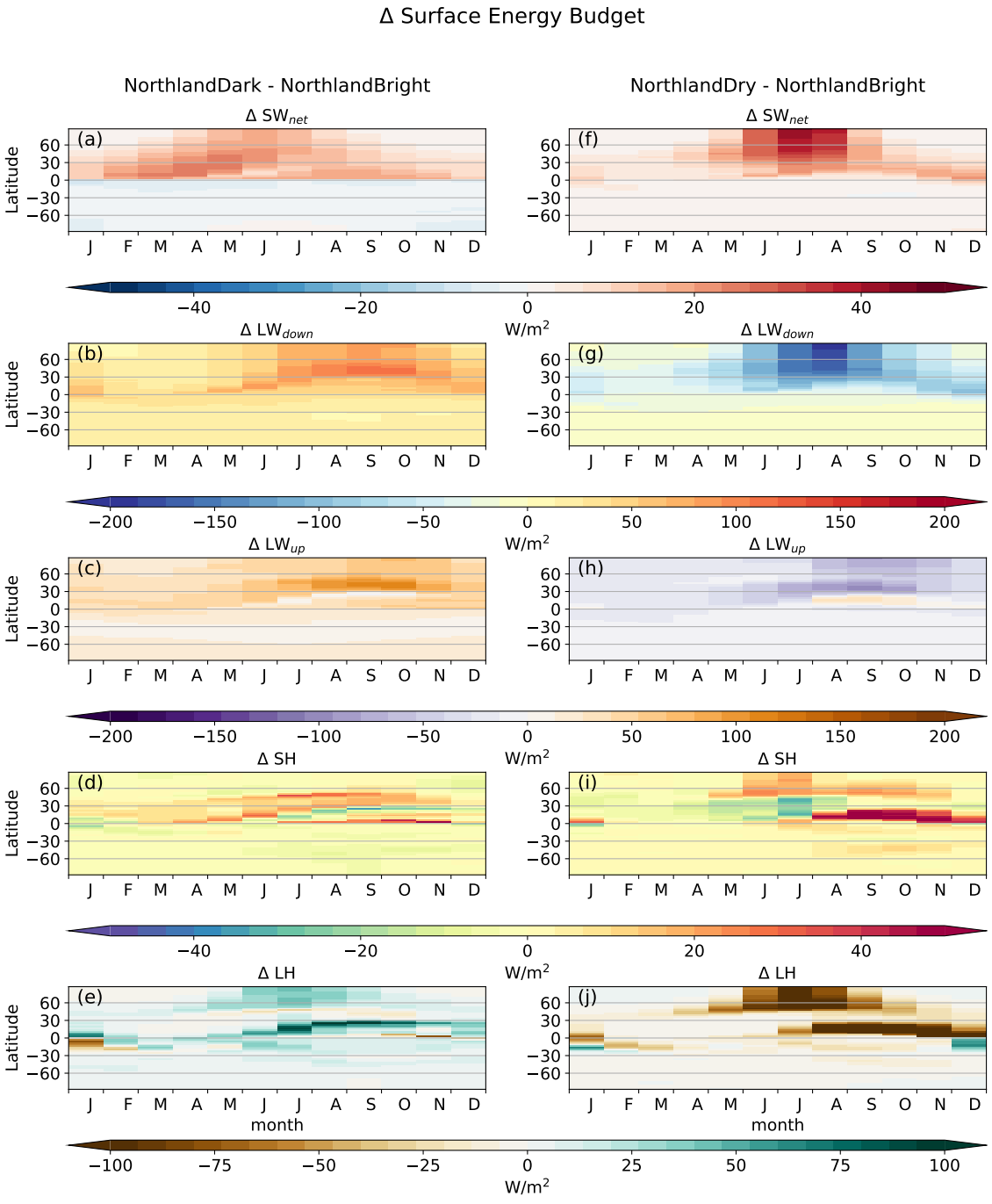

951 FIG. 3. Seasonal cycle of the change in zonal mean surface energy budget terms for NorthlandDark - North-
952 landBright (a-e) and NorthlandDry - NorthlandBright (f-j). Change in net surface shortwave radiation (a,f),
953 downwards longwave radiation (b,g), upwards longwave radiation (c,h), sensible heat flux (d,i), and latent heat
954 flux (e,j).

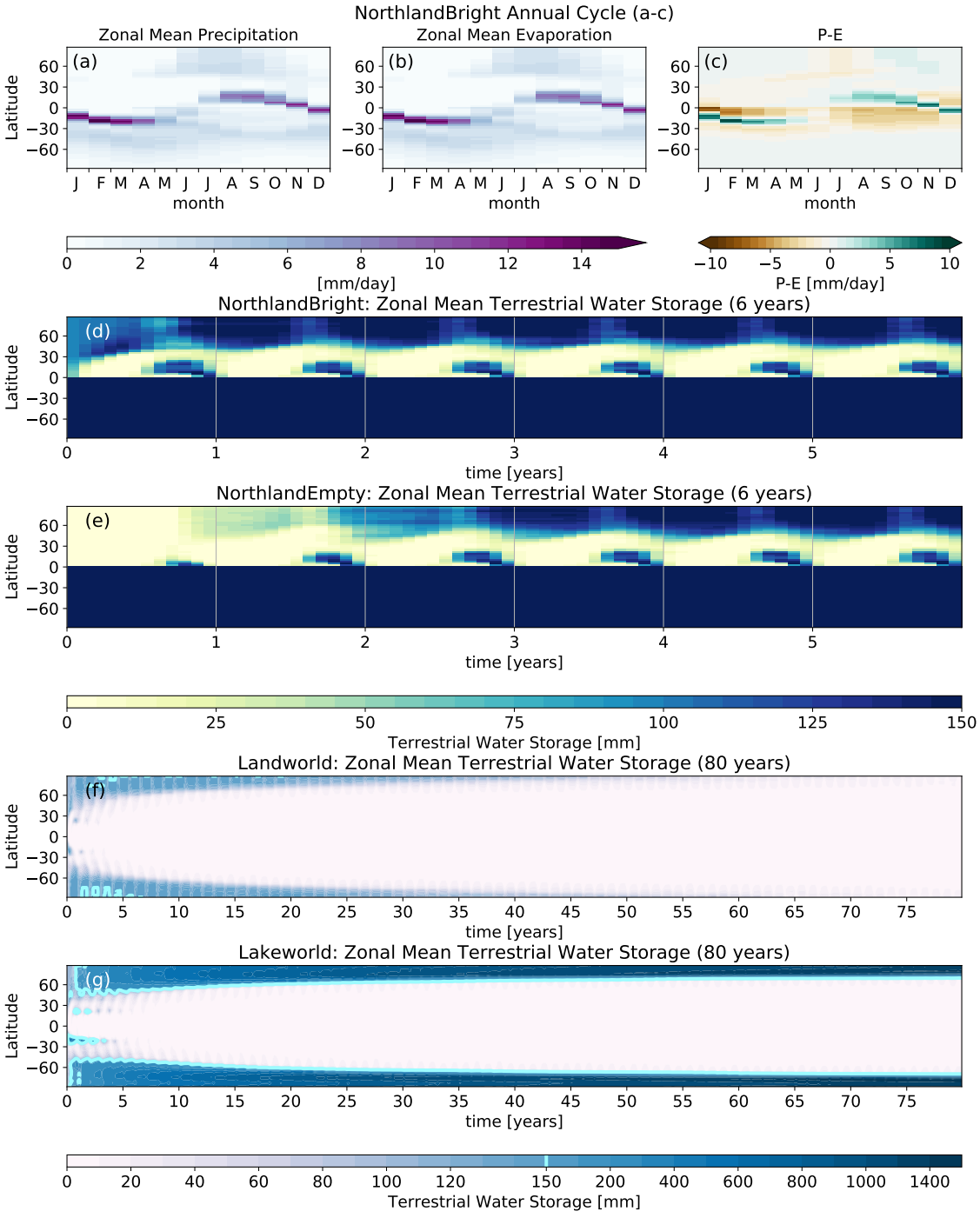

955 FIG. 4. Zonal mean seasonal cycle of (a) precipitation, (b) evaporation, and (c) precipitation-evaporation (P-
956 E) for the spun-up NorthlandBright simulation. Zonal mean terrestrial water storage over the first 6 simulation
957 years for (d) NorthlandBright and (e) NorthlandEmpty. Zonal mean terrestrial water storage for the full 80 year
958 simulations of (f) Landworld and (g) Lakeworld (note the non-linear colour bar). Cyan contour in (f,g) at 150mm
959 shows the bucket capacity (i.e. fully saturated soil moisture).

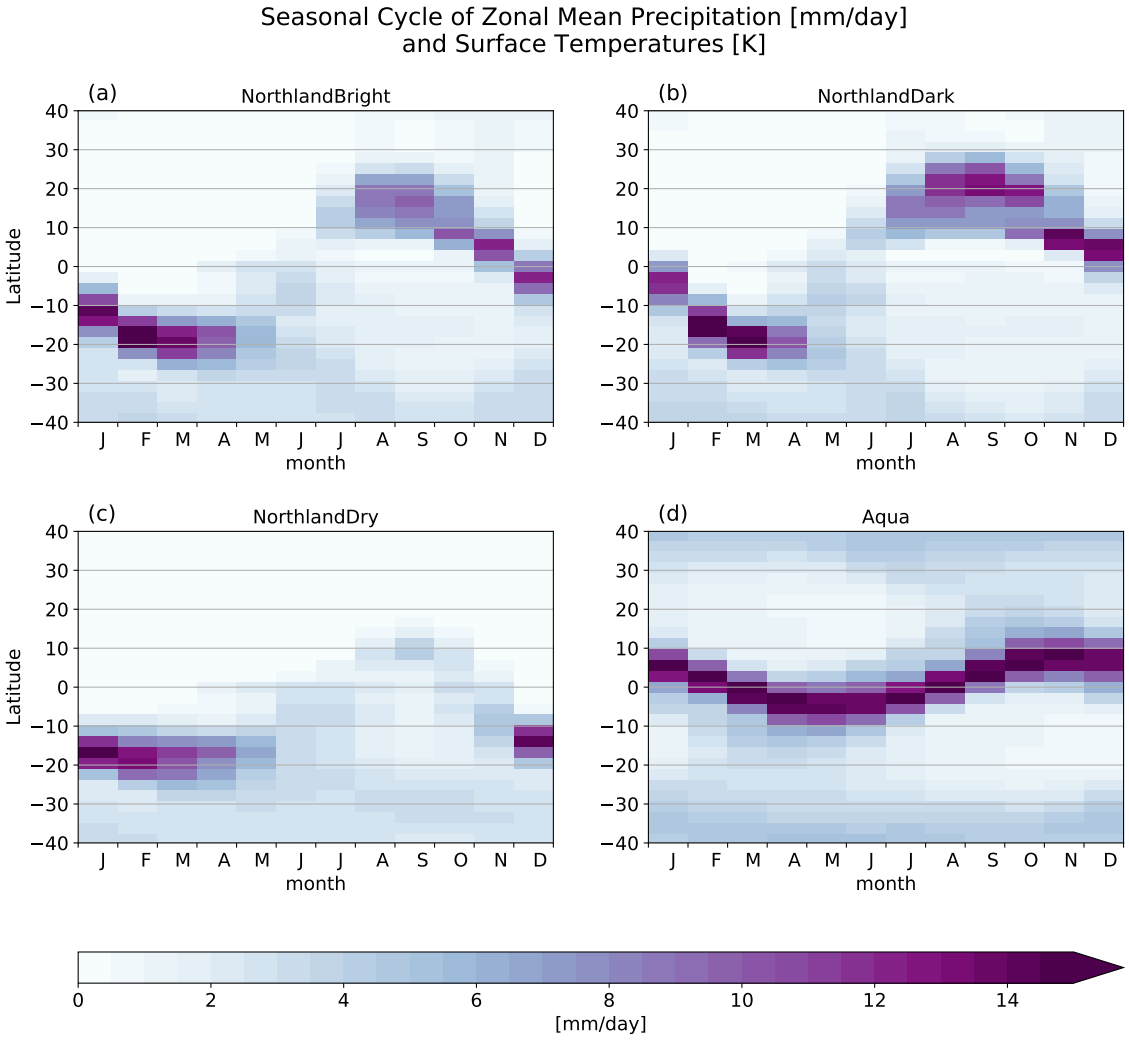

960 FIG. 5. Seasonal cycle of zonal mean precipitation from 40°S to 40°N in (a) NorthlandBright, (b) Northland-
961 Dark, (c) NorthlandDry, and (d) Aqua.

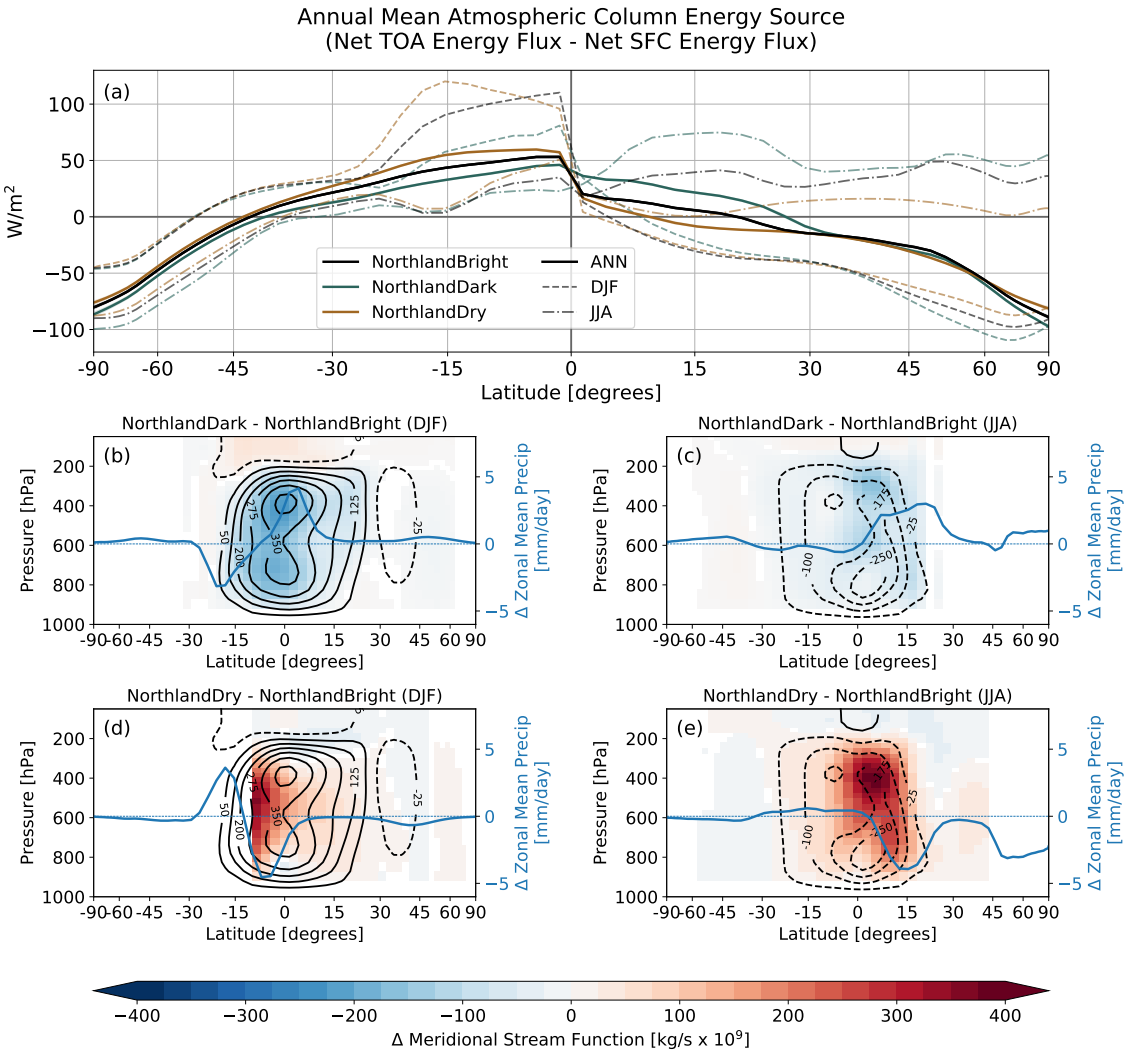

FIG. 6. (a) Zonal mean column energy source F_{net} for NorthlandBright (black), NorthlandDark (green), and NorthlandDry (brown) for the annual (black), JJA (red), and DJF (blue) mean. Contours in (b)-(e) show the NorthlandBright meridional stream function for DJF (b,d) and JJA (c,e), with shading showing the difference in the streamfunction between NorthlandDark-NorthlandBright (b,c) and NorthlandDry-NorthlandBright (d,e). Contour lines in b-d are spaced at 60×10^9 kg/s. The blue lines in (b)-(e) show the change in zonal mean precipitation. Panels (b,d) show DJF differences, while panels (c,e) show JJA differences. In panels (b-d), only values which differ significantly ($p < 0.05$ in a student's t-test) are shown.

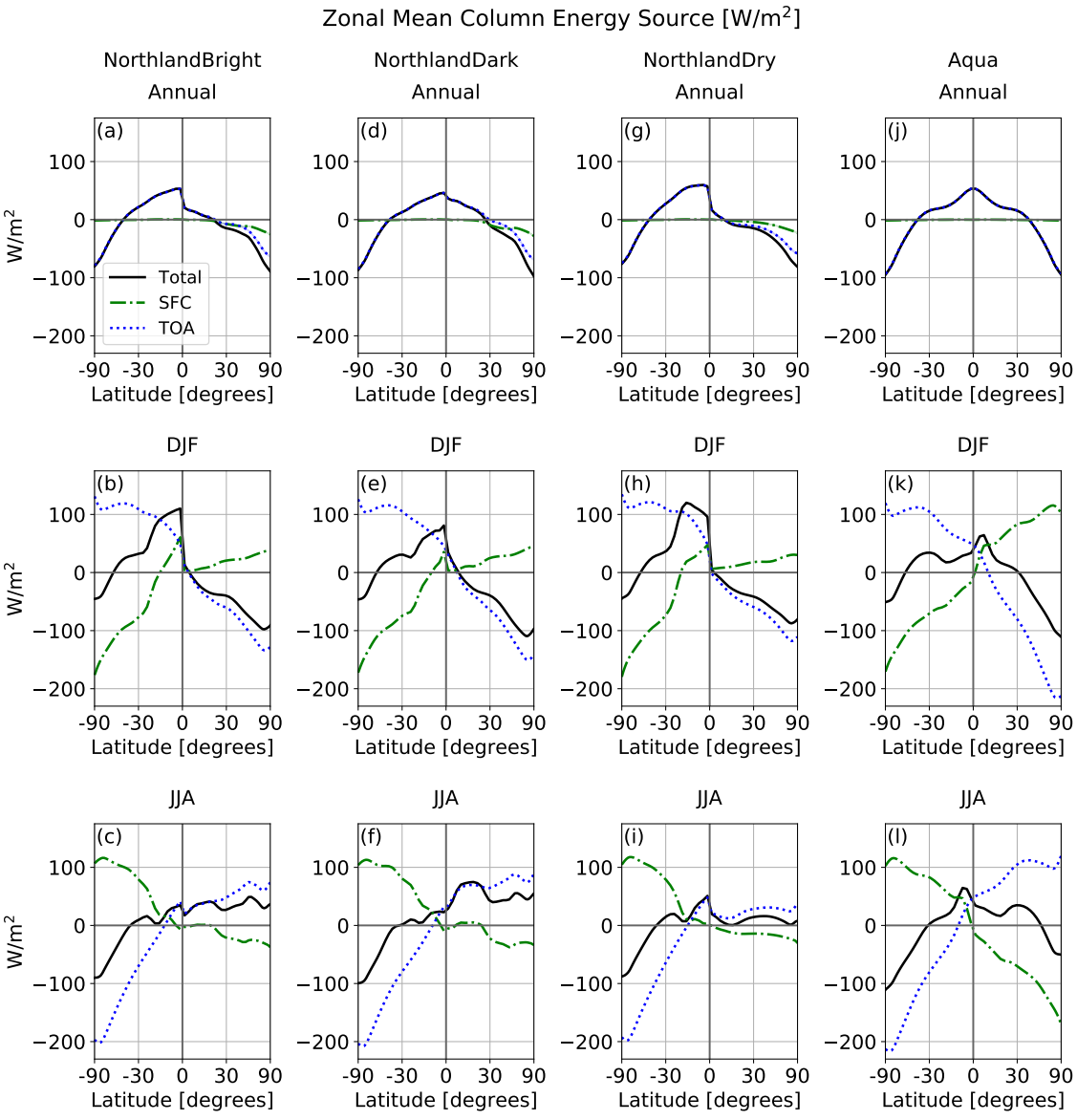

969 FIG. 7. Zonally averaged net TOA energy flux (blue dotted line), net surface energy flux (green dash-dot
970 line), and the atmospheric column energy source (TOA-SFC; black solid line) for the annual mean (top row),
971 DJF (middle row) and JJA (bottom row). NorthlandBright is shown in the first column, NorthlandDark in the
972 second, NorthlandDry in the third, and Aqua in the fourth.

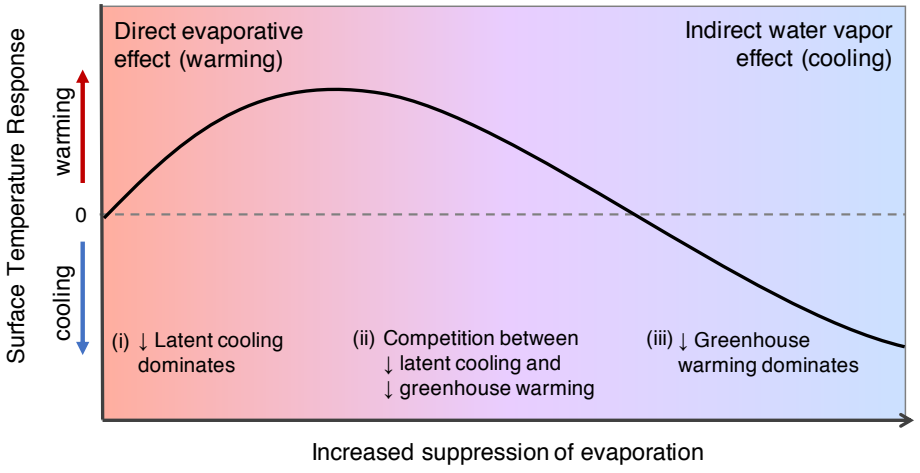

FIG. 8. Schematic showing the possible surface temperature response to decreased terrestrial evaporation.